AVL Simulation Tools
Practical Applications

Monografie – Politechnika Lubelska

Lublin University of Technology
Faculty of Mechanical Engineering
ul. Nadbystrzycka 36
20-618 LUBLIN

AVL Simulation Tools
Practical Applications

edited by
Łukasz Grabowski
Konrad Pietrykowski
Mirosław Wendeker

Politechnika Lubelska
Graz – Lublin 2012

Reviewers:
Prof. Eng. Rodolfo Taccani, University of Trieste (Italy)
Prof. Eng. Jerzy Merkisz, Poznan University of Technology (Poland)

Publication approved by the Rector of Lublin University of Technology

ISBN: 978-83-62596-89-8

Publisher: Lublin University of Technology
ul. Nadbystrzycka 38D, 20-618 Lublin, Poland
Realization: Lublin University of Technology Library
ul. Nadbystrzycka 36A, 20-618 Lublin, Poland
tel. (81) 538-46-59, email: wydawca@pollub.pl
www.biblioteka.pollub.pl
Printed by: TOP Agnieszka Łuczak
www.agencjatop.pl

Impression: 100 copies

Contents

Nomenclature

CAD Computer Aided Design
CFD Computational Fluid Dynamics
CI Compression Ignition
CNG Compressed Natural Gas
FEM Finite Element Method
HHO hydrogen and oxygen mixture which is a product of an electrolyse
LPG Liquified Petrolum Gas
PID Proportional-Integral-Derivative controller
PWM Pulse-Width Modulation
TDC Top Dead Center
SI Spark Ignition
ºCA Crankshaft Angle Degree

AVL FIRE & BOOST

AVL FIRE

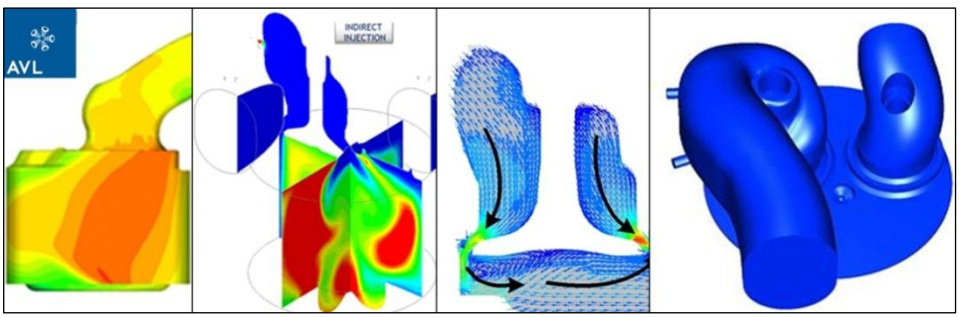

For more than two decades AVL FIRE has been used successfully in research and development departments of leading engineering companies to design and optimise internal combustion engines in terms of thermo-fluid dynamics. AVL itself maintains a team of 25 people who perform CFD simulation as customer service and as service within in-house research projects. Besides the permanent development and improvement of numerical, physical and chemical simulation models, this project work, which is directly integrated into the actual engine design and development process, is the major contribution to creating reliable, accurate, and successful software and providing countless benefit.

AVL FIRE was developed to solve the most demanding flow problems with respect to geometric complexity, chemical and physical modelling. Beside all functionality that is offered in the FIRE General Purpose package, FIRE Engine comprises special capabilities and modules (as listed below) particularly designed for computing fluid flow problems related to internal combustion engines. This includes simulating in-cylinder phenomena such as gas exchange, fuel injection, mixture generation, combustion and emission formation, but also calculating flows in injection equipment, exhaust gas aftertreatment systems and coolant flows.

The FIRE IC Engine Physics and Chemistry Module contains all features and functions required to simulate relevant physical and chemical processes related internal combustion engines. The module includes the FIRE Spray, Wallfilm and Combustion Capabilities.

The FIRE Spray Capabilities provide a worldwide leading technology for the CFD simulation of fuel injection and mixture formation in all types of spark ignited and compression ignition engines. It includes more than twenty different

models for spray formation and propagation including advanced model capabilities related to spray primary and secondary break-up, droplet dispersion, collision and coalescence, single and multi-component fuel evaporation, and wall interaction.

The FIRE Wallfilm Capabilities enable simulation, analysis and optimization of liquid wallfilm build-up, propagation and evaporation, and spray / wall and spray / wallfilm interaction. The FIRE wallfilm models are capable of handling multi-component fuels.

The FIRE Combustion Capabilities are a comprehensive set of models of different levels of complexity for fast and easy analysis and optimization of ignition, combustion, and emission phenomena. For spark-ignition engines knocking combustion tendency can be assessed additionally. Eddy-Break-Up, Turbulent Flame Speed Closure, Coherent Flame and Transported Multi-Scalar PDF models are a sound basis for simulating homogeneous / inhomogeneous and stratified charge SI engine conditions. For analysis and optimization of compression ignition combustion systems, FIRE provides another well-validated set of models describing the individual processes of auto-ignition, combustion and pollutant formation. Eddy-Break-Up, Characteristic Time Scale and the state of the art ECFM-3Z model enable the optimization of the various injection and combustion system parameters. Advanced NO and soot formation / depletion models assist the engine development engineer in assessing the emission characteristics of different concepts.

The FIRE Aftertreatment Module offers a wide range of capabilities related to the simulation of flow, heat transfer and catalytic surface reactions for various types of aftertreatment devices. Three-way catalysts, NOx storage catalysts as well as Diesel particulate filters and SCR systems can be addressed by the generic models offered in that context. Multiple scalar transport, user defined reaction schemes and reaction rate coefficients as well as the direct access to the CHEMKIN thermo-chemistry database, offer unique flexibility to all engineering problems related to exhaust gas after- treatment simulation.

The FIRE Coupling Module 1D/3D enables simultaneous coupling of AVL FIRE and AVL Boost, AVL's one-dimensional engine gas dynamics and cycle simulation software. This capability especially enhances transient optimization of intake and exhaust systems with respect to flow and residual gas distribution. The Coupling Module 1D/3D furthermore allows coupling FIRE with GT Power and WAVE.

The FIRE Coupling Module CFD/FEA allows exchanging data with ABAQUS and other established FEM solvers. This functionality is a major prerequisite for reliable prediction of solid temperatures and thermal stresses related to water and air cooling system optimization.

The FIRE Eulerian Multiphase Module offers unique capabilities for simulating flow phenomena in various IC-engine injection devices, including non-linear cavitation effects, also taking into account needle movement.

The results of a fully three-dimensional multiphase injector flow simulation can be easily used as input for the spray propagation simulation via the Nozzle Flow Interface. The module has been recently extended by implementing an erosion model, enabling the prediction of wear due to cavitation.

Solution accuracy:

- pressure based segregated solution algorithm,
- first and second order accurate implicit time discretization schemes,
- first, second and third order accurate conservative and bounded differencing schemes,
- first and second order pressure correction,
- multiple turbulence models, subgrid scale stress models and enhanced wall treatment models,
- multiple choices of inlet, outlet and wall boundary conditions including such for trans- and supersonic flows,
- application oriented chemical and physical models such as for species transport, reaction and combustion, Lagrangian dispersed phase modelling, multiphase modelling, wallfilm, radiation, heat,
- transfer.

Making use of these models, AVL FIRE has proven to be highly accurate in numerous real life projects comparing simulation results with measured data for various test cases and under various test conditions.

Major benefits:

- model generation requires little effort,
- state-of-the-art solver technology and the scalable solver performance,
- pre-configured simulation control files ensuring proper model and model parameter choice,
- result analysis tailored to problems including highly complex transient chemical and physical processes.

Hence by using AVL FIRE, a trial-and-error approach to achieve results and tedious tuning to get correct results belongs to the past. There is also no need to worry that problems will prolong model generation or the solution procedure unexpectedly. Project turn-around-times are foreseeably short and result quality is the highest possible. This makes AVL FIRE ready for its productive use - whatever IC engine or engine subsystem related fluid flow simulation task you wish to perform.

The newly developed CAD Data Manager allows the most common native CAD formats to be directly imported. Computational models are created in the software's automated meshing environment FAME, reliably providing boundary fitted hexahedron-dominated high-quality grids. The solver GUI enables the user to quickly set-up and start a simulation. The integrated post-processor offers all functions required to perform result analysis: to explore options, to optimise solutions and to make decisions.

BOOST

BOOST is a simulation programme developed for the modelling of a complete engine. The code can simulate the entire engine cycle including combustion.

BOOST was created within AVL's department for applied thermodynamics. The task of engine analysis using thermodynamic measurements and calculations is of special importance. This is because it constitutes the base from which the knowledge of how to model an engine is acquired and is a prerequisite for performing other tasks.

BOOST offers:

- graphical user interface (GUI) based on Windows technology,
- interactive pre-processor including model editor for guided input of the required data,
- interactive post-processor for fast analysis of results and comparison with test bed data,
- extensive interactive context orientated help facility,
- efficient simulation based on one-dimensional treatment of pipe flow and advanced models of other engine components,
- provision to link user defined sub-routines to the BOOST – code (FORTRAN compiler required),
- animated display of pressure waves.

The intuitive BOOST GUI enables users with basic knowledge of engine cycle simulation techniques to take full advantage of all capabilities within a short period of time. Even novice users are in a position to solve simple problems after a brief training period. BOOST Support Team is close to you. Highly qualified support engineers are located around the world.

BOOST is a powerful and user friendly tool for steady state and transient engine performance analysis. It can be applied to a range of tasks including:

- comparison of various engine concepts,
- optimizing component geometry, e.g. inlet system, exhaust system, valve sizes etc. with respect to power output, torque and fuel consumption,
- optimization of valve timing and cam profiles,
- layout of supercharging systems,
- orifice noise optimization,
- evaluation of transient engine performance (acceleration / load pick up, deceleration / load drop) taking into account the entire powertrain and vehicle dynamics.

Main features:

- pipes and junctions: The gas composition at any location is determined by solving the conservation laws for each mass fraction. Unburned fuel, combustion products and pure air are all considered. Thus a correct treatment of EGR (exhaust gas recirculation) is ensured,
- perforated pipes: perforations in a pipe wall can be modelled by including a pipe within another pipe or a plenum,
- flow restrictions: various kinds of restrictions including check valves and rotary valves,
- system boundaries,
- plenums and crankcases,
- air cleaner and air cooler,
- turbo- / super charging:
  - single and multiple entry turbines,
  - variable geometry turbine,
  - gear driven turbocompressor,
  - power turbine,
  - positive displacement compressor (e.g. ROOTS blower),
  - electrically assisted turbo-charger,
  - internal, external waste gate,
- combustion models:
  - vibe function,
  - 2-zone vibe (NOx),
  - experimental burn rate input,
  - MCC f. Diesel (Mixing Controlled Combustion Model; NOx),
  - Fractal Combustion Model for Petrol Engines (NOx, HC, CO),
  - user subroutines for combustion or high pressure cycle (FORTRAN compiler required),
  - constant pressure,
  - constant volume,
- control functions:
  - ECU; BOOST internal engine control unit,
  - PID Controller,
  - MATLAB™/Simulink, API Interface, DLL and s-function. All 3 are available on Windows and UNIX.
- FIRE Link: in cases where the one dimensional treatment of the flow is not sufficient, provision is made for a link to AVL's 3D flow simulation code FIRE,
- User Defined Element Provision to link user defined subroutines to the BOOST-code (FORTRAN compiler required).

Different modes are available for the analysis of the calculation results:

- message analysis: the messages written by the programme during a run may be sorted according message type, element or crank angle,

- transient analysis: the average results of each cycle calculated may be displayed either versus cycle number or time,
- traces analysis: time resolved results of the last cycle simulated are displayed versus crank angle,
- series analysis: average results for each simulated variant are displayed versus main variation parameter,
- acoustic analysis: the sound pressure level is calculated at the specified microphone position versus frequency in dB or as overall sound pressure in dB (A).

All results may be compared to results of measurements or previous calculations. Furthermore, an animated presentation of selected calculation results is available. This also contributes to developing the optimum solution to the user's problem. The post processor PP2 assists with the preparation of reports.

The International Seminar "AVL Simulation Tools – Practical Applications"

The International Seminar "AVL Simulation Tools – Practical Applications" was held on May 3, 2011 at the AVL List GmbH headquarters in Graz (Austria). Attended by the representatives of the Advanced Simulation Technology Department, this seminar aimed at sharing the experience in using advanced simulation techniques and providing the solutions to the current problems of AVL FIRE and AVL BOOST based modelling in their ongoing R&D activities. The authors of this monograph presented the results of their project "Hydrogen supply in the Wankel engine".

The Department of Thermodynamics, Fluid Mechanics and Aviation Propulsion Systems started to collaborate with AVL List GmbH at the beginning of 2009 when the parties signed a partnership agreement on applying this software for R&D. In 2010, the Laboratory for Advanced Modelling of Flows was founded at the Faculty of Mechanical Engineering of Lublin University of Technology. The authors of this monograph used the software by AVL List GmbH, i.e. AVL FIRE and AVL BOOST to calculate and simulate flow phenomena typical of combustion engines. This monograph includes their seminar presentations and papers.

The opportunity of meeting with AVL employees who had developed this software which has been applied at Lublin University of Technology resulted in further cooperation between these institutions and sharing their experience in using this kind of software. The software of AVL BOOST and AVL FIRE is used to model engine parts and processes including combustion chambers, gas injectors, hydrogen pressure regulators, intake systems, flows through a throttle, dual-fuel diesel engine working processes, gas supply processes in a spark ignition engine.

Fig. 1. Dr. Gotthard Ph. Rainer, Vice President of Advanced Simulation Technology Department

Fig. 2. Representatives of the Advanced Simulation Technology Department

On May 4, 2011, Werner Moser, AVL Vice President, hosted the authors of this monograph in the R&D centre in Graz and showed them around it. AVL List GmbH is a global research leader in internal combustion engines, propulsion systems and passenger car acoustics. The company provides test houses with research equipment and collaborates with nearly all automotive companies. The Lublin University of Technology employees could broaden their knowledge and gain new experience on the latest advances in the global automotive industry thanks to visiting the most advanced combustion engine laboratories and test benches at AVL List GmbH.

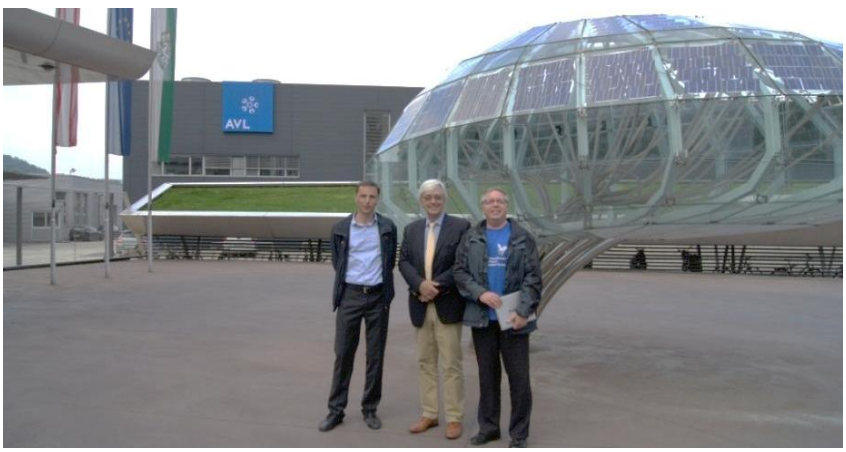

Fig. 3. Prof. Rodolfo Taccani, Werner Moser - AVL President, and prof. Mirosław Wendeker - AVL List GmbH headquarters in Graz

Fig. 4. Seminar participants

Mirosław WENDEKER

1. The simulation test of the flame front in the combustion chamber of the Wankel engine

Abstract

The AVL Fire-based model of the hydrogen combustion in a Wankel engine is described in this paper. Temperature distribution and the degree of charge combustion on a combustion chamber surface and in characteristic cross-sections are simulated. Additionally, emissions of toxic components for various values of the λ coefficient are analysed here.

Keywords: hydrogen, Wankel engine, AVL Fire, combustion

1.1. Introduction

A Wankel engine is a multi-purpose engine to drive aircraft, boats, motor vehicles or stationary devices. Its high specific power, simple construction, and small size are its main advantages. On the other hand, its drawbacks prevent from using liquid fuels such as petrol or a diesel fuel. A combustion chamber in a Wankel engine is very long and narrow so a flame cannot reach the most distant chamber parts. Thus, hydrogen seems to be a perfect fuel to power such engines. A hydrogen fuel features the much higher combustion rate so the whole charge can be burnt and the thermodynamic efficiency of combustion can significantly increase. The CFD modelling method helps to get a deeper insight into the heat release of the rotary engine in terms of temperature, the degree of charge combustion, the emissions of toxic components, and other parameters that impact on combustion.

1.2. CFD Modelling

Computational Fluid Dynamics allows a detailed approach to fluid flow and its related processes (heat and mass transfer, chemical reactions, etc.). Thus, it is necessary to build a discrete model, or a space that is divided into elementary finite volumes. Based on the finite volume method, CFD consists in solving differential equations of momentum, energy and mass balance using numerical methods.

Balances and boundary conditions need to be discretised to deal with the above issues. Thus, a system of nonlinear algebraic equations to describe transport for each computational cell is developed. Such a system can be solved

using a separable method (solving successive equations) or a total one (entire system of equations to be solved). This gives a system of linear algebraic equations where parameter values are calculated for cell centers; and central values should be interpolated to determine their values at walls.

A properly selected computational step is very important for correct calculations as it influences calculation accuracy and stability. After selecting a computational step, a computational cell size and gradients of fluid parameters in a model volume need to be considered.

1.3. Research object

Working on the Wankel principle, the Aixro XR50 has been selected for modelling. This single-rotor engine has got a maximum power of 33 kW, an eccentric shaft speed of 8,750 rpm. Its maximum torque is 39 Nm at 7,500 rpm and its chamber volume is 294 cm^3. Table 1.1 specifies *Aixro XR50*.

Tab. 1.1. Aixro XR50 - technical specification

type	4-stroke, single-rotor rotary engine
maximum power	33 kW at 8,750 rpm
weight	approx. 17 kg
maximum torque	39 Nm at 7,500 rpm
capacity	294 ccm
max. rpm	10,800 rpm
powering system	carburettor
ignition	full controled electronic system
cooling system	liquid

Fig. 1.1. AIXRO XR50

1.4. Model description

The geometry of the model developed in *Catia v5* comprises a combustion chamber confined by the surfaces of a piston and a cylinder. As the model of the surface is developed, it is entered into *AVL Fire* for digitizing. A computational meshgrid consists of about 90,000 cells, mainly *Hex* though *Tet* and *Pyramid.* The model view and the model itself with its computational grid are given in Figure 1.2 and 1.3, respectively. Due to the complex geometry of the piston movement in rotary engines, a fixed computing grid is used for the simulations which employ a standard k - ε turbulence model and a *Turbulence Flame Speed Closure* model. As one of numerous two-equation turbulence models, the standard $k-\varepsilon$ is the most common model used to calculate a low-speed incompressible fluid. The *TFSC* model is applied to determine the reaction rates related to turbulence parameters such as turbulence intensity, turbulent length scale, and flame structure parameters like flame front thickness and flame spread rate. Two mechanisms, i.e. self-ignition and flame spread determine the reaction rate.

Tab. 1.2. Boundary conditions

analysis type	crank-angle	**density**	1.19 kg/m^3
analysis module	combustion, charge transport	**temperature**	293.15 K
stroke	1^O CA	**turbulent kinetic energy**	0.001 m^2/s^2
analysis start	0^O CA	**turbulence**	k-ε
rotational velocity	1,000 rpm	**maximum iteration number**	20
pressure	100,000 Pa	**minimum iteration number**	1
ignition	spark	**result recording frequency**	1^O CA
ignition start	2^O CA	**combustion model**	TFSC
ignition duration	0.3 ms	**flame kernel diameter**	3 mm

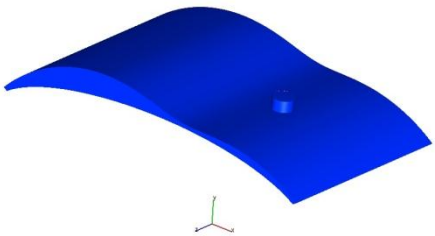

Fig. 1.2. Combustion chamber surface model

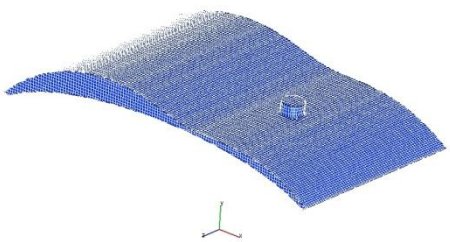

Fig. 1.3. Combustion chamber finite element grid

1.5. Results

The temperature distributions and degrees of charge combustion on the combustion chamber surface and in typical cross-sections within the spark plug socket have resulted from the simulations. The combustion of hydrogen for different values of the excess air coefficient λ is analysed. The combustion of petrol is simulated to compare the combustion courses. A step calculation is assumed to be at 1° CA. The results are recorded every 5° CA. The charts developed show the combustion as a function of the crank angle and emissions of toxic components, i.e. nitrogen oxides are only noticed for hydrogen combustion. Table 1.3 and 1.4 provide sample distributions of these values.

Tab. 1.3. Simulation results – temperature distribution

CA	Combustion chamber surface – temperature	
	hydrogen	petrol
20^0	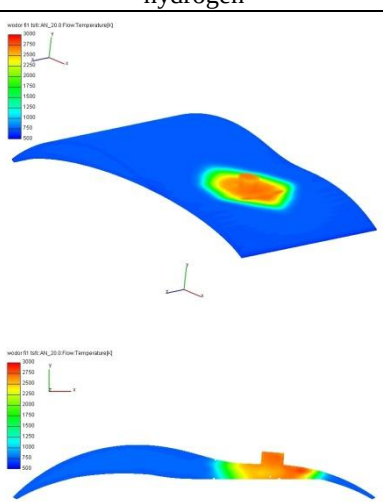	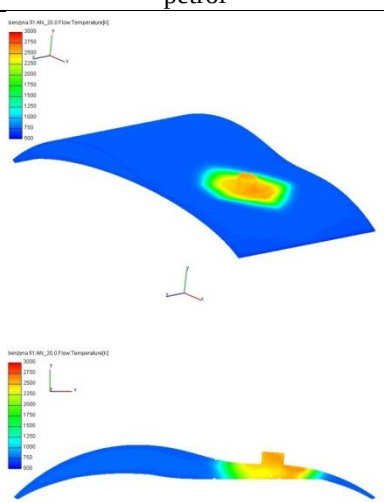

Tab. 1.3. Simulation results – temperature distribution – continued

45^0	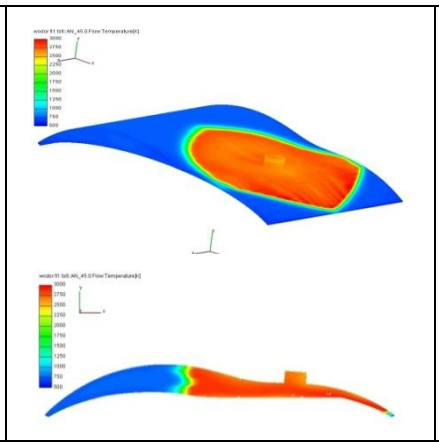	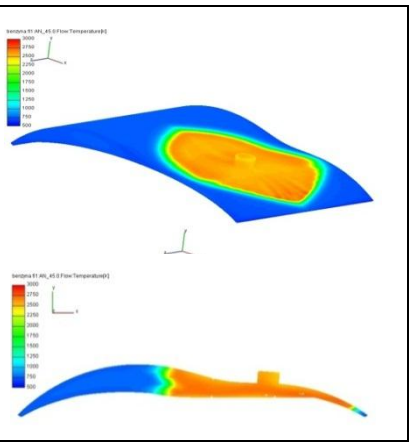

Tab. 1.4. Simulation results – combusted charge distribution

CA	Combustion chamber surface – combusted charge distribution	
	hydrogen	petrol
10^0	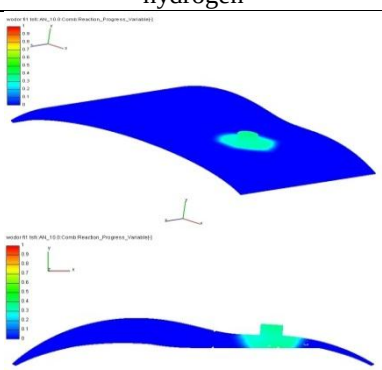	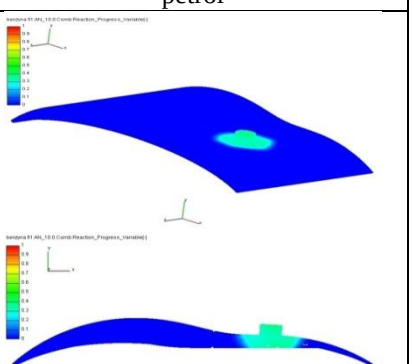
65^0	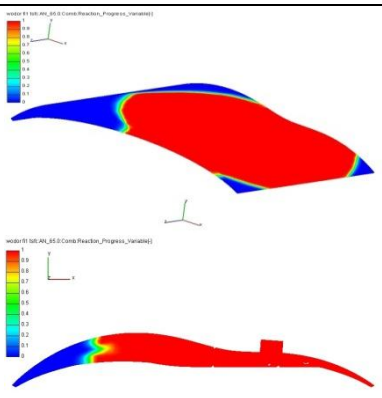	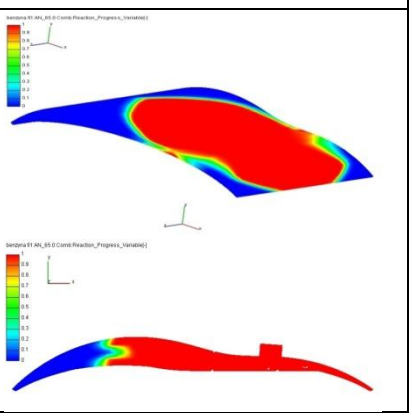

Based on these results, the hydrogen combustion in a Wankel engine can be analysed. The ignition starts at 2° CA though the first temperature change is recorded for 3° CA. When the ignition starts, a maximum temperature is about 1,500 K. For 10° CA, a flame comes out of a spark plug socket and spreads evenly in all directions. An increase in temperature and a consequent increase in the charge burn rate on the right side of the chamber are recorded in the next combustion phase. Higher temperatures occur inside the chamber, while at the walls they are much lower. A maximum temperature occurs just where the charge has already burnt out. For hydrogen, a combustion temperature is much higher and amounts to 3,000 K, whereas for petrol a maximum combustion temperature recorded is about 2,600 K. By analysing the degree of charge combustion, it can be concluded that hydrogen combustion proceeds much faster than that of petrol.

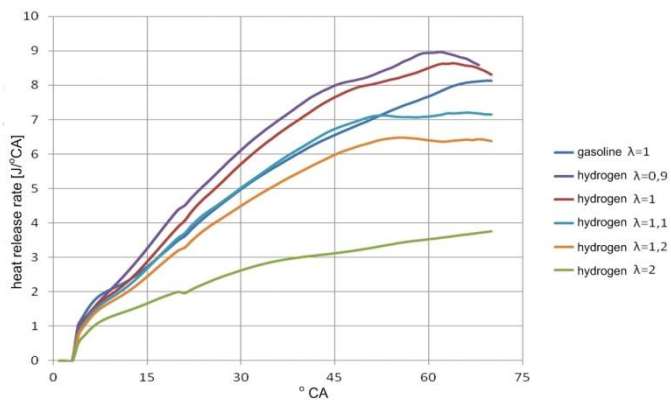

Fig. 1.4. Heat release rate for varied fuels and coefficient λ

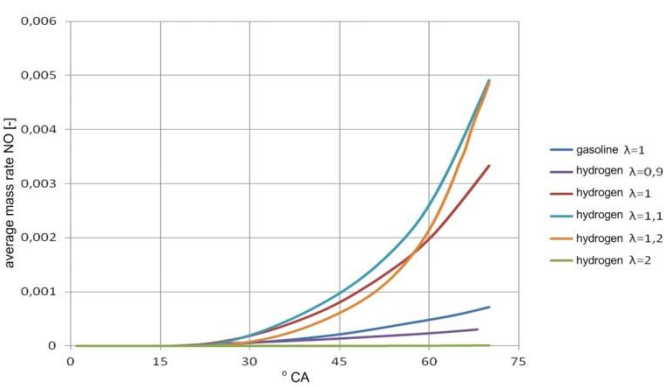

Fig. 1.5. NO_x average mass rate

The graphs in Figure 1.4 and 1.5 demonstrate the combustion of petrol and hydrogen for varied values of the excess air coefficient λ. Hydrogen combustion produces no toxic substances that contain carbon so the emissions of nitrogen oxides can be compared only. The simulations show that a hydrogen-air mixture for $\lambda = 2$ (lean mixture) contains less NOx as compared to the other mixtures tested. The highest average mass share of nitrogen oxides is recorded for mixtures of $\lambda = 1.1$ and $\lambda = 1.2$. For rich mixtures, the amount of nitrogen oxides decreases and for $\lambda = 0.9$ is smaller than that for the combustion of petrol. The analysis of the heat release rate shows that a mixture of $\lambda = 0.9$ has got the highest dynamics. For a mixture of $\lambda = 1.1$, the heat release rate is initially just as that of a petrol mixture and later it is slightly lower. A hydrogen mixture of $\lambda = 0.9$ (rich mixture) emits most heat.

1.6. Conclusion

AVL Fire programme based on computational fluid mechanics enables varied analyses, including those of combustion. Thus, the model developed can be used to accurately analyse the heat release in the Aixro XR50 Wankel engine, including the temperature distribution in the entire combustion chamber and the combustion itself. The combustion of petrol and hydrogen is analysed for the varied values of the excess air coefficient so that the combustion characteristics can be compared. Significant differences in the temperature distribution and degree of charge combustion are noticeable. Regarding emissions of toxic substances, an optimal mixture can also be determined based on these simulations.

References

[1] Gerke U.: *Numerical analysis of mixture formation and combustion in a hydrogen direct-injection internal combustion engine*. PhD thesis, Swiss Federal Institute of Technology, Zurich, Switzerland, 2007.

[2] Poojitganont T., Izweik H. T., Berg H. P.*: The Simulation of Flow Field inside the Wankel Combustion Chamber*, The 20th Conference of Mechanical Engineering Network of Thailand, Nakhon Ratchasima, Thailand, October 18–20, 2006.

[3] Izweik, H. T. *CFD Investigations of Mixture Formation, Flow and Combustion for Multi-Fuel Rotary Engine*. Ph.D. Dissertation, Brandenburg Technical University at Cottbus, Libya, 2009.

[4] Dinkelacker F., Hölzler S., Leipertz A.: *Studies with a Turbulent-Flame-Speed-Closure Model for Premixed Turbulent Flame Calculations*, 17th International Colloquium on the Dynamics of Explosions and Reactive Systems, Heidelberg, July 25-30, 1999.

Łukasz GRABOWSKI

2. The modelling of gas injector operation

Abstract

This paper discusses a new concept of an electronically controlled hydrogen injector for a multipoint injection system for a Wankel engine. This injector can be designed with the use of CFD (Computational Fluid Dynamics) methods, the AVL Fire software to optimise injector geometrical parameters, and magnetic field simulations to optimise an electromagnetic coil. Prototype injector test stand research, the current voltage and intensity in an electrical circuit are analysed to determine lag times for opening and closing an injector valve. Also, the impact of supply pressure for the operating parameters (opening time, closing time) and the pressure in an injector nozzle are analysed. Finally, injector flow characteristics as a function of injection time is developed.

The paper supports the hypothesis that the value of supply pressure can increase injector opening lag time. At the same time, higher supply pressure can decrease lag delay time for valve closing. The reference flow rate to ensure a proper supply in the Wankel engine tested has been achieved.

Keywords: Wankel engine, hydrogen, injector, CFD

2.1. Introduction

Current conventional energy resources are decreasing fast so people are trying to resort to alternative energy sources. The challenge for the automotive industry is to replace petroleum refined fuels with alternative ones. Hydrogen is a fuel that can satisfy all the requirements for alternative fuels; and its resources are almost limitless. Water is the only product of hydrogen burning. Hydrogen is a clean fuel, which is particularly important due to increasingly strict standards for emissions of toxic components. Nowadays, a system for sequential multipoint injection into an intake manifold is the most common type of a supply system for gaseous fuels in SI engines. This sort of supply system has been successfully used for LPG or CNG and it can be also used for hydrogen. This gas, however, shows several drawbacks such as very low density, susceptibility to spontaneous combustion or a very narrow gap for flame quenching. Consequently, using hydrogen in the supply systems of conventional engines can be really difficult. Hydrogen low density requires a large volume of gas to be supplied into a combustion chamber to ensure a correct fuel dose for efficient combustion. This implies the need of increasing supply overpressure and injection time or using several injectors for each cylinder. Although beneficial

for a higher level of charge burning, a narrow gap for flame quenching can cause unwanted backfiring in intake pipes. Thus, for hydrogen, the design of injectors as elements to directly provide fuel into intake pipes should be adapted for higher pressures that occur in a supply system and a necessary and significant increase in the volume flow rate, where relevant operating parameters are maintained, i.e. timing for valve opening or closing. An injector should also have a linear flow rate characteristics as a function of injection timing and operation repeatability.

Supplying the Wankel engine with hydrogen is very profitable due to some undeniable advantages of this kind of engine. The use of this fuel is facilitated mainly by separating a combustion zone from a mixture formation zone, which almost prevents from some unfavorable phenomena like knocking or backfiring in intake pipes.

This paper presents a new concept of an electronically controlled hydrogen injector system designed for a multi-point indirect injection ideal for Wankel engines. The simulation studies deal with the medium flow inside injectors, the magnetic induction distribution in a coil assembly and a real model test to verify injector operating parameters.

2.2. Injector model

The injector consists of two elements which constitute an assembly housing. The first element, i.e. electromagnetic coil housing includes also a pipe to supply a working medium and a pipe to distribute a gas into an injector manifold. To obtain a very high volume flow rate, the injector assembly comprises two subcomponents. The main element to control injector operation is a cylindrical core with an additional surface perpendicular to its axis. An elastic element to seal an outlet valve is on this surface. A resilient element to support valve closing is between the coil and the magnetic circuit. Replaceable outlet connections fixed into the lower housing allow adjusting the injector flow rate by changing a nozzle diameter. The injector operates on the impulse dosing of fuel into an intake pipe. When no current flows in the magnetic circuit, the control piston and the sealing element rest on the injection nozzle inlet due to the force produced by the resilient element and prevent the outflow of the gas from the injector. When an electric current starts flowing, an electromagnetic field occurs and attracts the piston which acts as a coil armature for a magnetic circuit, and as a result, this sealing element shifts from the injector nozzle and the working medium flows out of the device as shown in Figure 2.1.

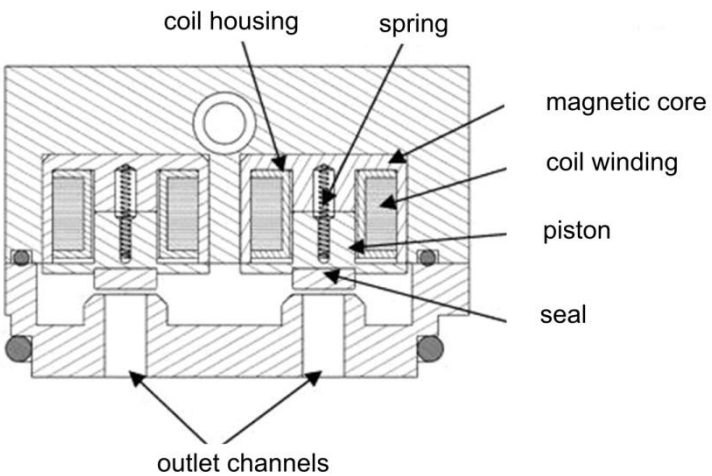

Fig. 2.1. Injector cross-section

2.3. Simulation tests

Optimizing a device design needs CFD simulations with *AVL Fire* to select the best configuration for individual elements of the injector. These simulations have helped select an optimum pipe configuration to distribute the working medium into the collective chamber and to guarantee the best injector operation. The tests are based on a CAD model as shown in Figure 2.2.

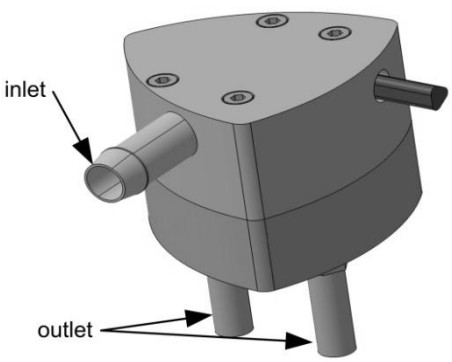

Fig. 2.2. CAD model for the injector

The simulation studies are carried out for four pipe configuration options. Therefore, models for the injector interior for each configuration are required. The two options of the inlet and outlet pipe configuration are given in Figure 2.3.

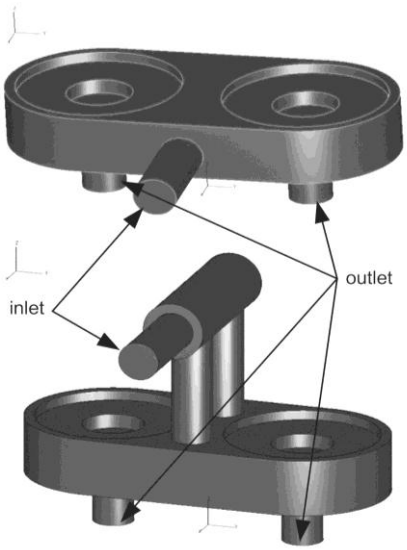

Fig. 2.3. Tested configurations of the injector pipes

The boundary conditions for the simulation are as follows:

- analysis type: *steady*,
- pressure:
  - inlet: constant static pressure of 400 kPa,
  - outlet: static pressure of 100 kPa,
- turbulence model: *k-zeta-f*,
- compressible working medium.

The simulations have determined the impact of the geometry of the pipes, i.e. intake, outlet, and to distribute the working medium, on velocity and pressure distribution. The results of the simulations are shown in Figures 2.4-2.9. The results include also the distribution of streamlines where the values for velocity and pressure are identified (Fig. 2.6, 2.9). The studies show that the way an intake pipe is placed influences the pressure and velocity distribution in an injector collective chamber. Also, the working medium is noted to swirl in a varied manner. The injector model with a single inlet pipe mounted above the collective chamber and two pipes to distribute a medium features a uniform pressure and velocity distribution in the outlet area. The highest pressure drops occur at the entrance to the outlet nozzle and the medium flows fastest just there. In the chamber, there are no adverse phenomena like medium turbulence which could negatively influence the medium as it flows towards the exhaust nozzles. The working medium in the nozzle outlet reaches a maximum velocity of about 420 m/s and its maximum pressure in the outlet pipe is about 250 kPa. These values are lower for other configurations.

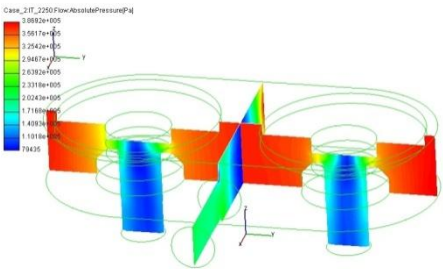

Fig. 2.4. Pressure in the characteristic cross-sections

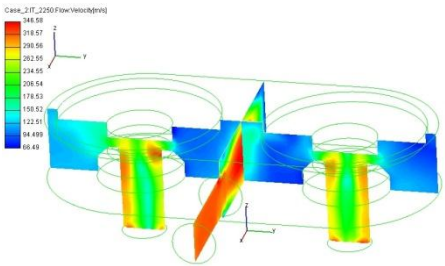

Fig. 2.5. Velocity in the characteristic cross-sections

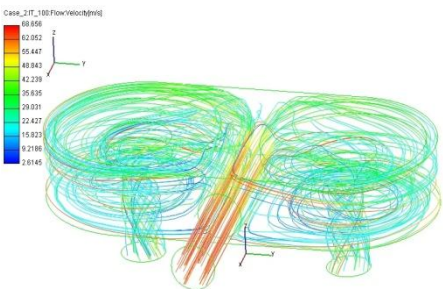

Fig. 2.6. Streamlines with the velocity values

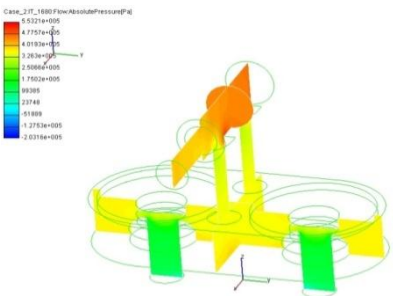

Fig. 2.7. Pressure in the characteristic cross-sections

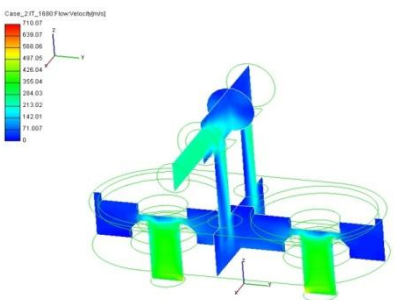

Fig. 2.8. Velocity in the characteristic cross-sections

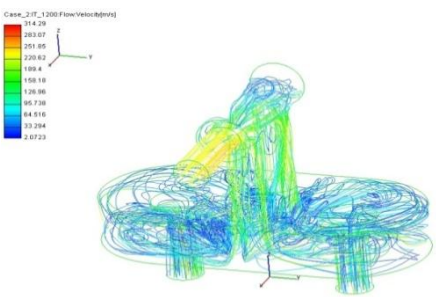

Fig. 2.9. Streamlines with the velocity values

The simulations of a magnetic field are to optimise the geometry of the electromagnet components and to obtain the most favorable operating parameters. The tests are performed using *Quick field*, simulation software based on the finite element method (FEM), to determine magnetic field distribution for the reference coil parameters. This software facilitates the determination of magnetic field lines and magnetic field induction for the reference conditions for supplying the coil. The study verifies the effect of the geometrical parameters of the coil subcomponents and the shape of the controlling piston as a coil armature on the value of the force generated. The coil wire diameter is 0.3 mm for the initial calculation. The coil resistance is about 2 Ω. Figure 2.10 shows the distribution of magnetic induction and the magnetic field lines for the selected geometries for a coil and a control piston.

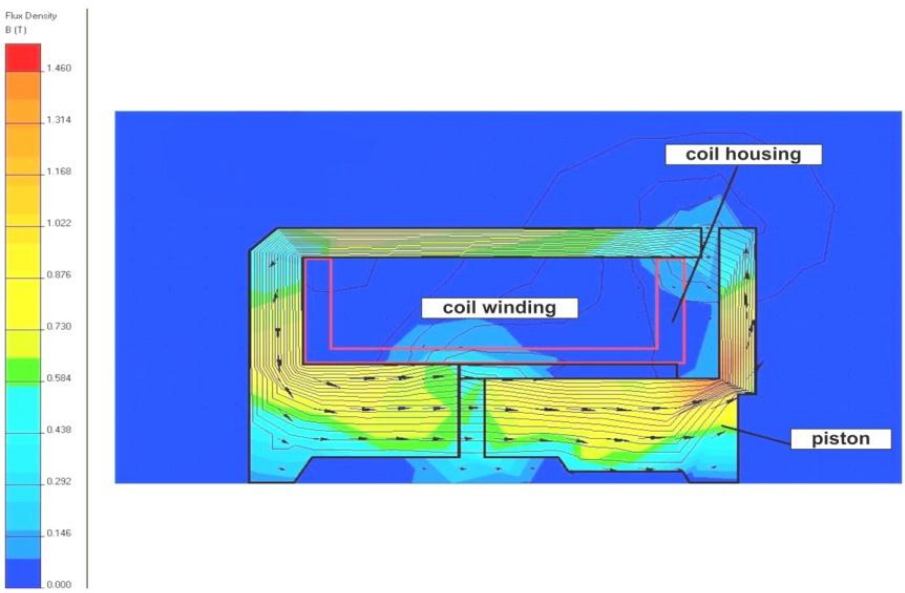

Fig. 2.10. Magnetic induction and magnetic field lines

2.4. Injector research

The study allowed optimizing the injector design and making its real model. Figure 2.11 shows all the components of the device.

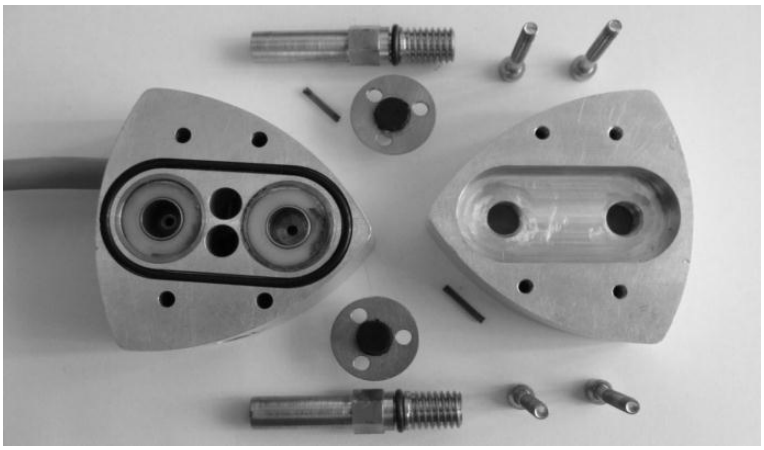

Fig. 2.11. Injector components

The injector model is tested on a test stand dedicated for specifying operating parameters of gas injectors. Compressed air is a working medium; and the test stand includes a compressor with a tank of compressed air, an air drying system with a pressure regulator, and a control system to control an injector. The test stand also includes:

- an air flow meter to determine the volume flow rate of outflowing air,
- MPX4250 air pressure sensor mounted at the outlet to specify lag time for injector closing (and a system to measure voltage of a current flowing in a circuit),
- a current probe to measure an electric current flowing in a circuit to determine lag time for injector opening.

An oscilloscope is used to read the results. Figure 2.12 shows the test stand scheme.

The intensity and voltage of the current flowing in the injector circuit as well as the voltage from the pressure sensor mounted at the outlet valve of the injector are recorded during the tests. These parameters enable specifying injector opening and closing times. Also, the air flow meter mounted at the injector outlet provides the values to develop the characteristics of the volume flow rate in the injector as a function of its opening time. The study refers to the following values of supply overpressure: 200, 300, 400, and 500 kPa. Additionally, a constant injector activation time of 3 ms and a 30% duty cycle PWM are determined.

The values for the current intensity in the circuit are used to specify lag time for injector opening for different values of supply overpressure. The values for outlet injector pressure and the current voltage enable specifying lag time for valve closing. The sample of an oscilloscope screenshot is in Figure 2.13.

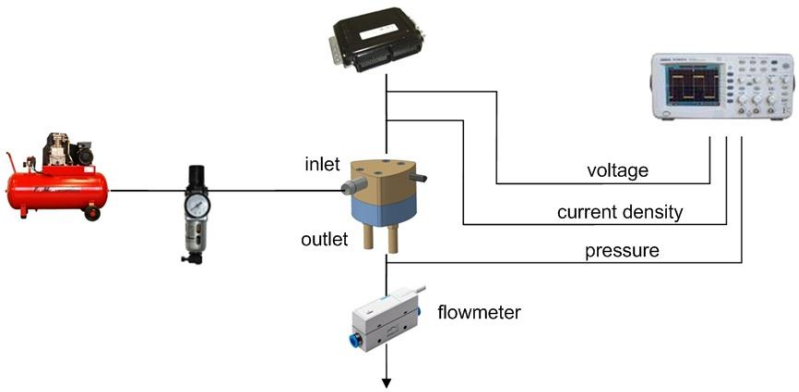

Fig. 2.12. Scheme of the test stand

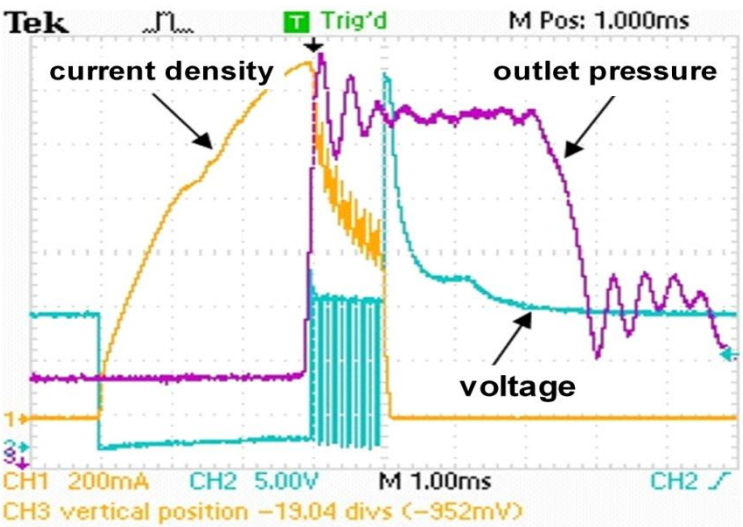

Fig. 2.13. Screenshot of the oscilloscope

Based on the research, the impact of supply overpressure on the main injector operating parameters such as lag time for valve opening and closing has been determined. These parameters, in turn, are used to specify outlet injector pressure changes in relation to supply overpressure. Figure 2.14 shows the impact of the supply overpressure on the lag time for valve opening.

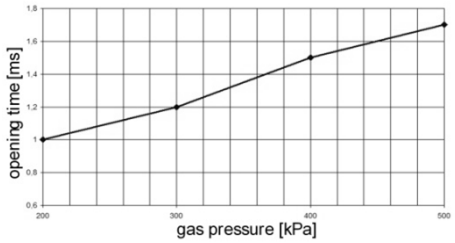

Fig. 2.14. Lag time for full valve opening depends on supply overpressure

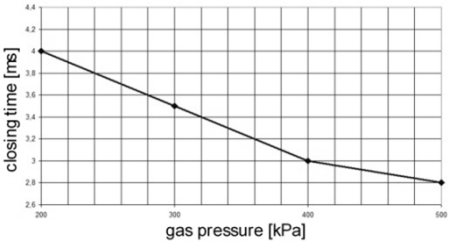

Fig. 2.15. Lag time for valve closing depends on supply overpressure

The higher values of the supply overpressure in the tested injector supply system are reflected in the higher lag time for injector opening. The higher lag time for valve opening is related to the higher drag force due to the medium pressure. For a supply overpressure of 200 kPa, a lag time for full valve opening is 1 ms, whereas for the maximum overpressure adopted for the tests, a lag time for injector opening is 1.7 ms. The increased supply overpressure is negative for the lag time for full valve opening, but the increased overpressure is positive for the lag time for valve closing (Fig. 2.15). This lag time, however, is much larger compared to the lag time for opening, which may be caused by a too weak force generated by the resilient element.

The study also results in making an injector volume flow rate characteristics as a function of injection time for the reference values of supply overpressure. The characteristics are shown in Figure 2.16. The characteristics are for a supply overpressure ranging from 200 kPa to 500 kPa. These characteristics show perfectly injector operation, i.e. injector opening time is shorter than its closing time by about 1 ms (for a 500 kPa supply overpressure), which can be confirmed by setting the intersection of this characteristics with Y-axis. Also, all the characteristics for the entire operation are linear, which means a stable operation regardless of injection time and facilitates a fuel injection control. No significant disturbances in the characteristics for the reference supply overpressure are noted. The flow rate required for proper engine supplying is achieved. However, it is obtained only at a 500 kPa supply overpressure. The injector flow rate can be increased by means of injection nozzles of a larger diameter or an increased stroke of a piston that controls valve opening and closing. The latter, however, may deteriorate device parameters, e.g. to increase lag time for valve opening, which may hinder an optimal injector control for shorter injection times.

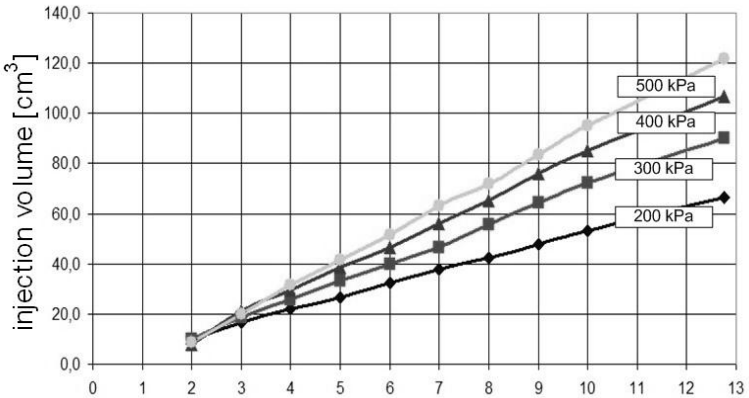

Fig. 2.16. Injector characteristics

2.5. Summary

The concept of an electronically controlled hydrogen injector for the Wankel engine is developed with advanced CAD systems. These tools optimise the geometries of device individual components before a real model is made.

The studies have confirmed the proper operation of the device. The operation characteristics for all the values of supply overpressure is linear. The injector volume flow rate obtained is as required. Since this device meets all of the assumptions, it can be a good basis to develop this design further.

References

[1] Hydrogen properties. Module 1, *Hydrogen fuel cell engines and related technologies*. College of Desert; Revision O, December 2001.

[2] Verhelst S., Wallner T.: *Hydrogen-fueled internal combustion engines*, Progress in Energy and Combustion Science 35 (2009).

[3] Escalante Soberanis M. A., Fernandez A. M.: *A review on the technical adaptations for internal combustion engines to operate with gas/hydrogen mixtures*, International Journal of Hydrogen Energy (2009) 1–7.

[4] Wendeker M., Jakliński P., Grabowski Ł., Pietrykowski K., Czarnigowski J., Hunicz J.: *Model klapowego wtryskiwacza CNG do silników spalinowych*, Silniki spalinowe PTNSS-2007-SS4-223.

Grzegorz BARAŃSKI, Ksenia SIADKOWSKA

3. The simulation of the hydrogen pressure regulator

Abstract

This paper focuses on a design and simulation and experimental results regarding a prototype of an electronically controlled hydrogen pressure regulator. The geometric CAD (Computer Aided Design) model of the regulator has been developed using the Catia v5 software. This model has been developed based on the mass demand for a hydrogen fuel in the Wankel engine under research. Done with the use of the Ansys Fluent software, the simulation research employs a CFD method. The simulations can determine the impact of regulator geometrical parameters like a nozzle geometry, a size of nozzle chambers and a high and reduced pressure on its basic flow parameters, i.e. velocity and pressure distribution. The experimental tests on this prototype pressure regulator are done under operating conditions in an automotive vehicle. Basically, the study verifies a system response to a control error, i.e. verifies regulator operation with respect to its output pressure stability.

The paper shows the non-uniform distribution of medium pressure and velocity in a hydrogen pressure regulator with different nozzle types. The real model of a pressure regulator with a single-hole nozzle has resulted from the simulation tests. The optimal sizing of chambers, a nozzle shape, and an electronic control system for hydrogen pressure confirm that the prototype hydrogen pressure regulator stabilises the pressure on target.

Keywords: hydrogen, pressure, electronic control, experimental tests, CFD

3.1. Introduction

Nowadays, people are frequently searching for cheaper and cleaner energy sources to supply combustion engines and are attempting to replace petrol and diesel fuels with various fuels that have combustion less harmful to the environment. Petrol is replaced with fuels such as methane, a mixture of propane and butane, alcohols; whereas esters of rapeseed or palm oil can be used instead of a diesel fuel. Increasingly, hydrogen is used to power internal combustion engines. Exhaust gases from burning a mixture of hydrogen and oxygen contain no CO_2 which causes a greenhouse effect. Unfortunately, transport and storage of liquid or gaseous hydrogen are tough tasks.

Before reaching an intake manifold or a combustion chamber regardless of an engine type, hydrogen fuel pressure needs to be decreased to nominal

operating conditions of a supply system, i.e. nominal operating pressure of supply actuators, or injectors. Thus, a pressure regulator maintains constant pressure and necessary flow intensity between high pressure hydrogen tanks and a low pressure supply system. This device stabilises the pressure in a supply system when engine power changes upon changing a fuel dose supplied to an engine. Also, such a regulator should thermally stabilise a medium flowing through it.

A regulator design should ensure a smooth and steeples control of the medium flow rate. An innovative method to regulate the initial parameters of the tested pressure regulator for hydrogen means a combination of a classical membrane regulator and a solenoid electronic control system which can maintain constant medium pressure. An electronic system for pulse width modulation (PWM) is controlled with a proportional-integral-derivative controller (PID controller) within a closed feedback loop. Such a precise control of opening time for a solenoid valve enables the smooth and steeples adjusting of a regulator flow rate for current engine fuel demand.

3.2. Research on the hydrogen pressure regulator

3.2.1. Design assumptions

The hydrogen pressure regulator is a single-step electronically controlled membrane pressure regulator (Fig. 3.1 and 3.3). The device controls the amount of a flowing medium and thermally stabilises gas pressure at a constant and assumed level. Compressed hydrogen (its selected properties are in Table 3.1) is a working medium for the research regulator.

Tab. 3.1. Comparison of the selected properties of hydrogen and petrol

parameter	hydrogen	petrol	unit
density	0.0899	775	kg/m^3
heating value	120.1	43.5	MJ/kg
octane number	130	91-100	-
min. ignition energy	0.02	0.24	mJ
ignition temperature	858	501	K
air combustion rate	0.265–0.235	0.37–0.43	m/s

From a battery of hydrogen tanks, the hydrogen is supplied at a 1.0 MPa pressure to the regulator where its pressure is reduced to 0.4 MPa. Later, the medium is transported along pipes to the engine supply system and actuators, i.e. gas injectors.

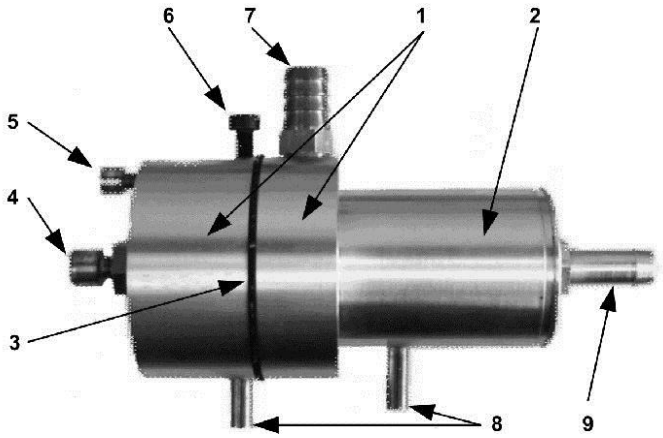

Fig. 3.1. View of the hydrogen pressure regulator, 1 – high pressure chamber, 2 – reduced pressure chamber, 3 – membrane, 4 – screw for adjusting the volume of the high pressure chamber, 5 – screw for the regulating nozzle, 6 – pressure sensor connection, 7 – medium inlet, 8 – solenoid connection, 9 – medium outlet

Made of light alloy materials, the hydrogen pressure regulator consists of two bodies separated by a receptive and regulating element, or a membrane. The body of the reduced pressure chamber (body on the right in Figure 3.1) forms a part of a high pressure chamber and a reduced pressure chamber. Both chambers are separated by a main nozzle (see Figure 3.2.a).

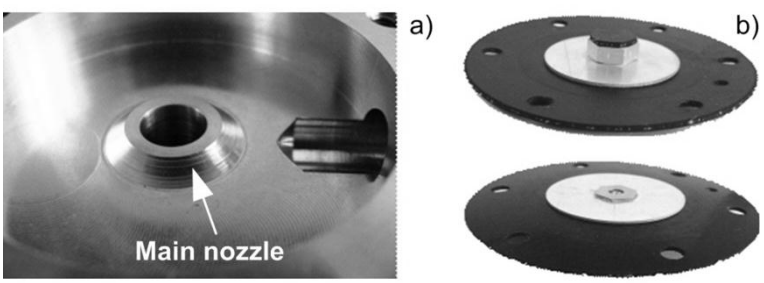

Fig. 3.2. Pressure regulator components, a) high pressure chamber, b) membrane

The second part of the body, i.e. “under the membrane” (on the left in Figure 3.1) forms another part of the high pressure chamber. The parts of the high pressure chamber, i.e. "over the membrane and below the membrane" are connected with the regulating nozzle, while the high and reduced pressure chambers are connected to the electronic solenoid valve by means of the main nozzle and the side channel.

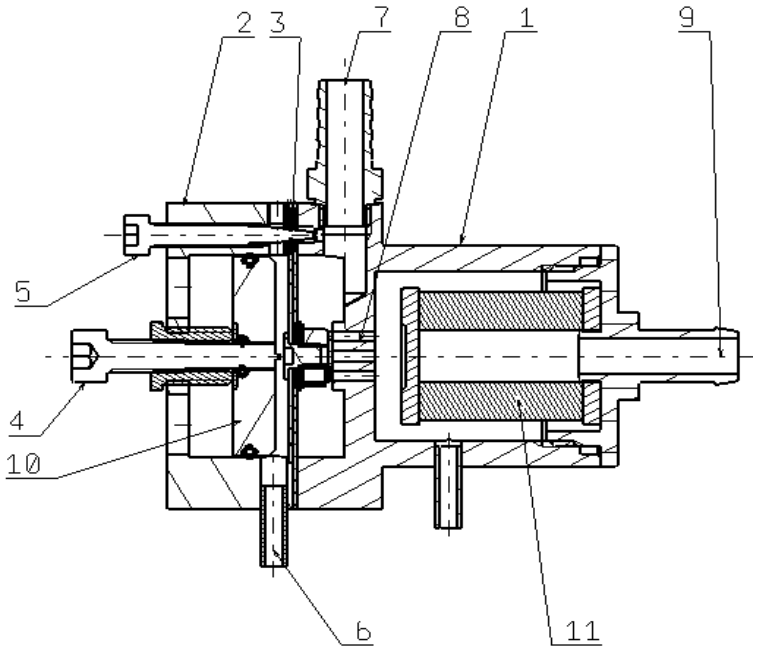

Fig. 3.3. Longitudinal section of the test hydrogen pressure regulator, 1 – reduced pressure chamber, 2 – high pressure chamber, 3 – membrane, 4 – screw to adjust the volume in the high pressure chamber, 5 – regulating nozzle screw, 6 – solenoid connection, 7 – inlet, 8 – main nozzle, 9 – outlet, 10 – movable wall in the high pressure chamber

The element to limit the cross-section of the main nozzle when the medium flows from the high pressure chamber to the reduced pressure chamber is attached to the membrane. The medium reaches the high pressure chamber through the inlet connector, i.e. calibrated regulating nozzle and applies pressure on the both sides of the regulator membrane. The different pressures above and below the membrane deform the membrane so that the nozzle opens or closes. After increasing the cross-section of the nozzle, the medium flows into the reduced pressure chamber and decompresses. Later, the medium flows towards the regulator outlet connector and engine supply system. A difference in membrane surface pressure is attained by decreasing ”the under-the-membrane pressure” in the high pressure chamber. A pressure drop is due to starting up the solenoid valve and depleting the medium from the high pressure chamber to the reduced pressure chamber.

The solenoid valve is controlled with the PWM system, i.e. solenoid valve opening and the PID controller within a closed loop (determining a control error).

3.2.2. Simulations

The simulation of the flow and velocities of the medium in the pressure regulator is done with Ansys Fluent 13.0 which is based on CFD. The simulations help specify the impact of the geometry of the main nozzle pipes in the regulator and the size of the main regulator "above-the-membrane" space upon basic flow parameters like velocity or pressure distribution.

The geometric model for the regulator is developed in Catia v5 (Figure 3.4.a). The model is based on the Wankel engine mass demand for hydrogen fuel. The simulation employs two regulator models developed, i.e. having a single-hole nozzle (Figure 3.4.b) and a multiple-hole nozzle (Figure 3.4.c). The former has got an active nozzle cross-section area of 50.265 mm^2, whereas the latter has got 7 holes of the same total cross-sectional area.

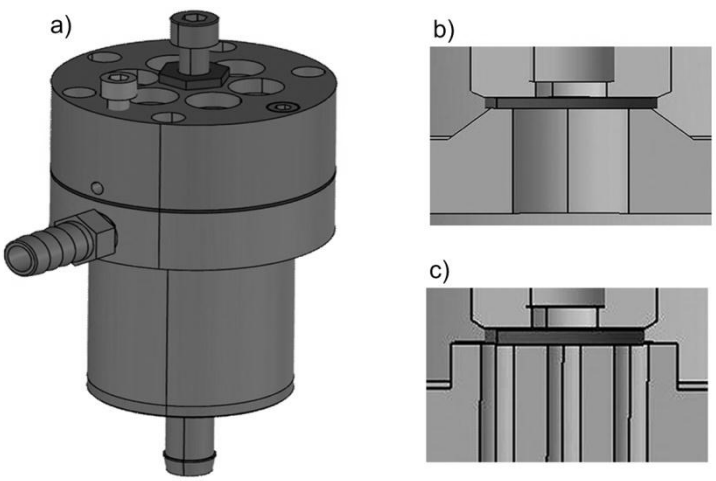

Fig. 3.4. Geometric model of the pressure regulator, a) general view, b) longitudinal section for the single-hole nozzle, c) longitudinal section for the multiple-hole nozzle

The model computing grid is generated using Ansys Fluent 13.0. The grid consists of 24,250 cells (5,061 nodes) for the single-hole nozzle regulator model (Figure 3.5) and 40,712 cells (9,209 nodes) for the multiple-hole nozzle regulator model (Figure 3.6). To speed up the simulations, a function of symmetry is used, i.e. a symmetric half model is developed to be symmetrically reflected by means of this programme.

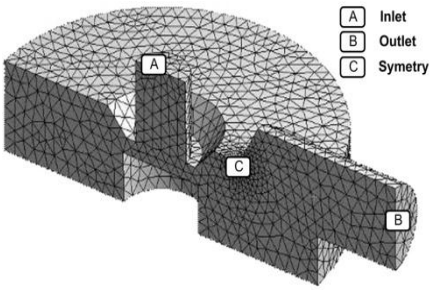

Fig. 3.5. Grid model for the operating space of the single-hole nozzle pressure regulator

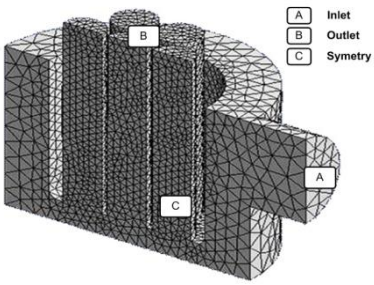

Fig. 3.6. Grid model for the operating space of the multiple-hole nozzle pressure regulator

The initial conditions are as follows:

- inlet pressure – 1.0 MPa,
- outlet pressure – 0.4 MPa.

For the regulator model is tested under sensitive operation conditions, constant inlet and outlet pressure is set.

The simulation parameters are as follows:

- analysis type: steady state,
- flux type: laminar,
- pressure – 0.3 MPa;
- analysis start: ranges from zero to the reference inlet value.

The results of the simulations are shown in Figures 3.7. to 3.12.

Having stabilised the flow in the multiple-hole nozzle regulator, the greatest backpressure is in the high pressure chamber, opposite the medium inlet (marked red and orange in Figure 3.12). Clearly, pressure differences are between each nozzle pipe. The discrepancy largely results in the non-uniform flow through each nozzle pipe.

The velocity of gas flowing through the single-hole nozzle pressure regulator is 0 m/s at the walls and is as high as about 860 m/s if nearer to the nozzle symmetry axis.

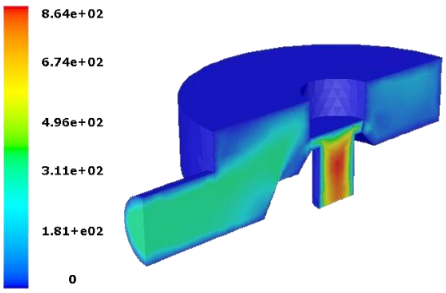

Fig. 3.7. Simulation results for the velocity [m/s] in the single-hole nozzle regulator

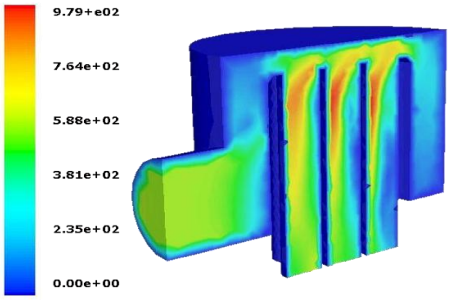

Fig. 3.8. Simulation results for the velocity [m/s] in the multiple-hole nozzle regulator

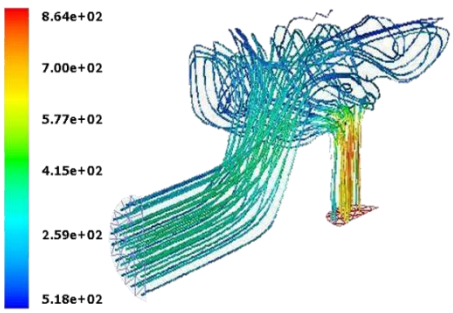

Fig. 3.9. Mapping of the current streamlines [m/s] in the single-hole nozzle regulator

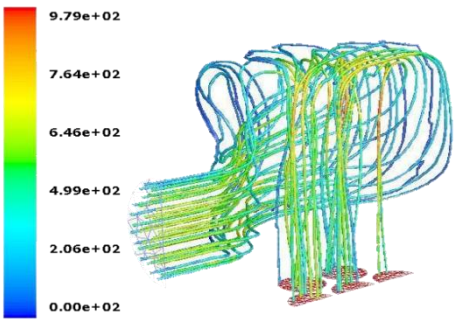

Fig. 3.10. Mapping of the current streamlines [m/s] in the multiple-hole nozzle regulator

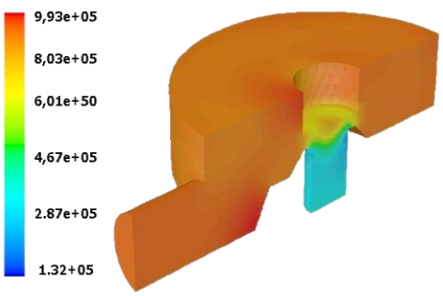

Fig. 3.11. Simulating the pressure distribution [Pa] in the single-hole nozzle regulator

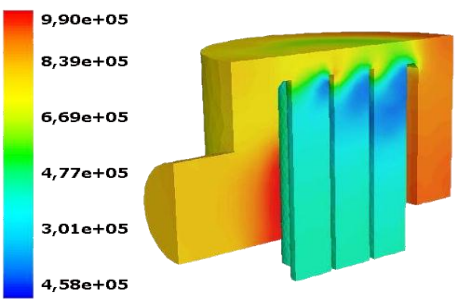

Fig. 3.12. Simulating the pressure distribution [Pa] in the multiple-hole nozzle regulator

3.2.3. Experiments

Carried out on an automotive vehicle under operating conditions, the experiments verify a system response to the quantity of a control error, or verify regulator operation for its outlet pressure stability.

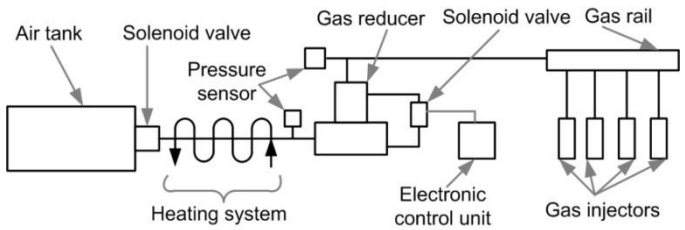

Fig. 3.13. Schematic of the measuring system for the pressure regulator

The measuring system to test the pressure regulator (Figure 3.13) was designed to dose the medium from the high pressure fuel tank to the actuators, i.e. gas injectors. If the solenoid valve is activated, i.e. opened, the medium accumulated in the tank flows into the regulator where the pressure is reduced to the reference pressure value. Then, the reduced and steady pressure medium flows into the fuel tank from which it is dosed to the gas injectors. The medium pressure is measured by pressure sensors at two points, i.e. in front of and behind the regulator.

The study is done for two different thermodynamic states of the medium, i.e. pressure and temperature. The temperature and pressure of the flowing medium changes because the medium is heated (convection) by a heater installed between the gas tank and the regulator. The study is done for the heating system turned on and off. The results of the experimental studies are shown in Figures 3.14. to 3.16.

As shown in Figure 3.14, the mean outlet pressure is 0.2 MPa and it oscillates around this value with a relatively small amplitude (curve p_2). The amplitude largely depends on the variation and degree of engine load, fuel demand variation, and the control system used in the pressure regulator. The magnitude of changes in an engine demand for fuel should not significantly affect the change in outlet regulator pressure if a regulator design, a regulating method, and reference parameters are correctly selected.

Using the PID controller within a closed feedback loop allows a control error to approach 0, which means obtaining a reduced and constant set medium pressure (here the pressure is 0.2 MPa). The PID controller controls opening the solenoid valve of the regulator injector by selecting the optimal value of PWM regulator output pulse width. The higher engine fuel demand is, the more the PID controller can increase a PWM filling coefficient, which shows the PWM curve in Figure 3.14.

For the changes in pressure above 0.15 MPa at the input, a control lag is quite significant. Consequently, the regulator output pressure differs from the reference pressure. This fact is reflected in the changes in pressure and PWM regulator as regulator outlet pressure peaks (extreme), which is shown by curve p_2 in Figure 3.14).

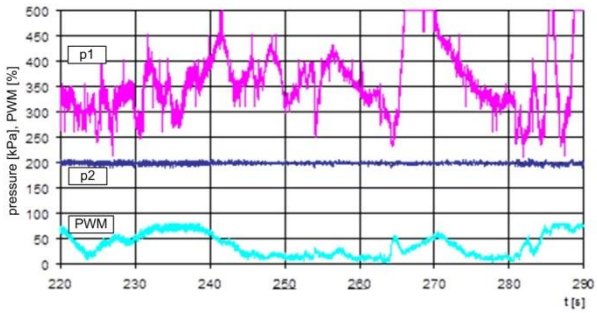

Fig. 3.14. The course of pressure regulator and PWM test pressure during the experimental, p_1 – pressure curve of the power regulator, p_2 – pressure curve at the outlet of the regulator, *PWM* – pulse width modulation curve

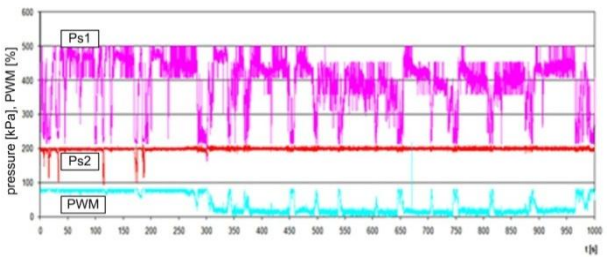

Fig. 3.15. The changes in pressure and PWM regulator pressure with the disabled heating system, *Ps1* – pressure before the tested regulator, *Ps2* – pressure behind the tested regulator

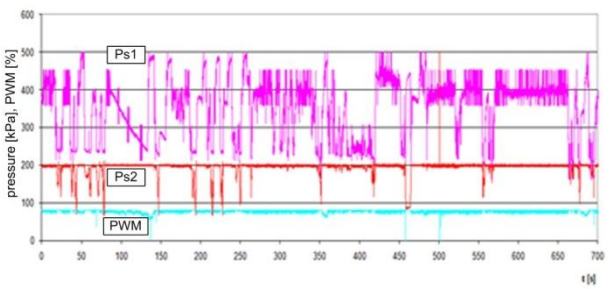

Fig. 3.16. The changes in pressure and PWM regulator pressure with the enabled heating system, *Ps1* – pressure before the tested regulator, *Ps2* – pressure behind the tested regulator

Figure 3.15 and 3.16 show the pressure regulator operation with the disabled and enabled heating system. The use of the heating system do not influence much the volume of the pressure regulated. The change in system operating conditions, engine fuel demand, and regulator supply pressure indicates that the regulator operation is stable and its reference pressure of 0.2 MPa is maintained.

3.3. Conclusion

Based on the simulation studies, pressure distribution between nozzle pipes varies for the single-hole pressure regulator. This pressure discrepancy influences how much medium can flow though each nozzle pipe. The medium may stop flowing in nozzle pipes that are most distant from the main inlet. For a single-hole nozzle, the pressure is evenly distributed on the entire nozzle cross-section, whereas velocity distribution behaves in compliance with a laminar flow velocity profile.

The simulation studies resulted in developing a real pressure regulator. Due to no uniformity of the flowing medium through each pipe of the multi-hole nozzle regulator and varied medium velocities in different parts, the pressure regulator with a multiple-hole nozzle will not be analysed any longer. The uniformity of pressure distribution and optimum velocity distribution in the single-hole nozzle resulted in developing a prototype pressure regulator with a single-hole nozzle.

The studies on the electronically controlled pressure regulator with a single-hole nozzle have shown that the prototype hydrogen pressure regulator maintains a reference pressure constant. Any sudden changes in pressure in the supply system do not disturb the regulator operation as the regulator can quite quickly adapt to new operating conditions.

References

[1] Lanz A., Eng P., Heffel J., Messer C.: *Hydrogen properties*. Published by College of the Desert, Palm Desert, CA, USA Energy Technology Training Center Rev., December 2001.

[2] Lanz A., Eng P., Heffel J., Messer C.: *Hydrogen use in internal combustion engine*. Published by College of the Desert, Palm Desert, CA, USA Energy Technology Training Center Rev., December 2001.

[3] Hari Ganeshb R., Subramaniana V., Balasubramanianb V., Mallikarjunaa J. M, Ramesha A., Sharmaa R. P.: *Hydrogen fueled spark ignition engine with electronically controlled manifold injection: An experimental study*. Renewable energy, 2008.

[4] Wright P. S., Pickering J. R.: *An AC Voltage Standard Based on a PWM DAC,* IEEE transactions on instrumentation and measurement, 48(2), April 1999.

Konrad PIETRYKOWSKI

4. The calculation of the airflow through the intake system of the Wankel engine

Abstract

This paper reports the results from the CFD simulation on the hydrogen injection into the Wankel engine intake manifold. This research specifies the distribution of a hydrogen fuel in an intake manifold for different injector installations. The tests determine the distributions of pressure, velocity and mass flow. It has been demonstrated that the correct fuel distribution in an intake manifold is only for the two variants of hydrogen injector installation. The calculations have been done with the use of AVL Fire.

Keywords: injection, hydrogen, intake system, experimental tests, CFD

4.1. Introduction

Modifying an intake system in a hydrogen-powered Wankel engine includes the phenomena that occur in an intake manifold under engine operation. Two geometrical factors condition the way a Wankel engine is filled with an air-fuel mixture, i.e. an intake manifold design and a place where a hydrogen injector is mounted. Computational fluid dynamics (CFD) techniques allow for analysing the phenomena that occur in an intake system.

Volumetric efficiency is one of the most common parameters to be applied while designing internal combustion engines. It is defined as a ratio of the mass of the medium that is actually supplied to a combustion chamber and the mass of the medium that is held in a total volume of a combustion chamber. It is, therefore, so important to develop an appropriate design of an inlet system [4], [5].

The way a gas injector is arranged relative to an intake valve axis can significantly influence engine operation, which is confirmed by the measurements of toxic component concentrations in exhaust gases [2]. The increased toxicity of exhaust gases as a result of mounting a gas injection nozzle more distantly is due to deteriorated combustion [1], [3].

CFD is a very effective tool to optimise engine designing [6]. This technique enables such an intake system design that can ensure an effective engine filling and a testing of different hydrogen injector installation options.

4.2. Objective

The objective is to develop certain modifications for the Wankel engine intake system design. These modifications cover the flow phenomena that occur in an intake manifold. Consequently, a model of an intake system is developed in AVL Fire. The simulations are performed using numerical fluid mechanics which is a method to verify any assumptions regarding a Wankel engine intake system. Due to the nature of engine operation, i.e. under stationary conditions (see Figure 4.1) an intake system should precisely control a mass airflow rate.

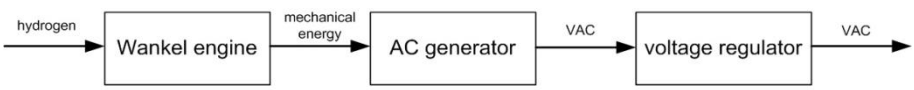

Fig. 4.1. Block diagram of a system to generate electricity

An intake system design has a significant impact on how an engine is filled with a mixture. If an engine is fuelled with hydrogen, there is no fuel deposition on intake manifold walls just as an engine is fuelled with petrol. In fact, a fuel supply point is meaningful. If an injector is mounted in a correct way, engine volumetric efficiency and appropriate mixture distribution between two intake ducts are provided. *AVL Fire* is used to simulate hydrogen injection. The simulation steps are as follows:

- pre-processing includes any activities necessary to start numerical calculations, i.e. developing a geometric model and a grid (discretization in space), defining boundary conditions, initial conditions, and gas and its parameters;
- a solver enables calculations in system discrete point generated with required discretization time from a computing grid. A solver also deals with, e.g. gas mixing, an ideal gas density model, turbulent flow phenomena;
- post-processing consists in presenting results diagrammatically. Relevant diagrams show quantities analysed for a given area.

4.3. Inlet system geometric model

A geometric model of the intake system (Figure 4.2) is developed in CATIA v5. Its dimensions are based on the author's own measurements and design documentation available. In addition, the injector is within the adapter geometry developed.

Fig. 4.2. Geometric model

This digitised intake model is done with *AVL Fire*. The geometric model, i.e. surfaces and edges is imported into this programme. The next step involves defining a cell type. Calculation efficiency and accuracy are closely related to the quality of the grid generated. A geometric discretization error decreases with decreasing grid density, as specified in the principle of *Cn*, where *C* is a grid density coefficient and *n* is approximate scheme accuracy. To avoid discontinuities in this geometry and to ensure the required accuracy of calculations, the correctness of the grid developed is verified using a special function in this software. The model consists of approximately 100,000 cells. Such geometric discretization can ensure the accuracy required while reducing computational time. This numerical model is based on the author's own research.

The basic model specification is shown in the table below.

Tab. 4.1. Model specification

cells	103,254
knots	105,606
total surface area	0.022 m^2
total volume	0.00013 m^3

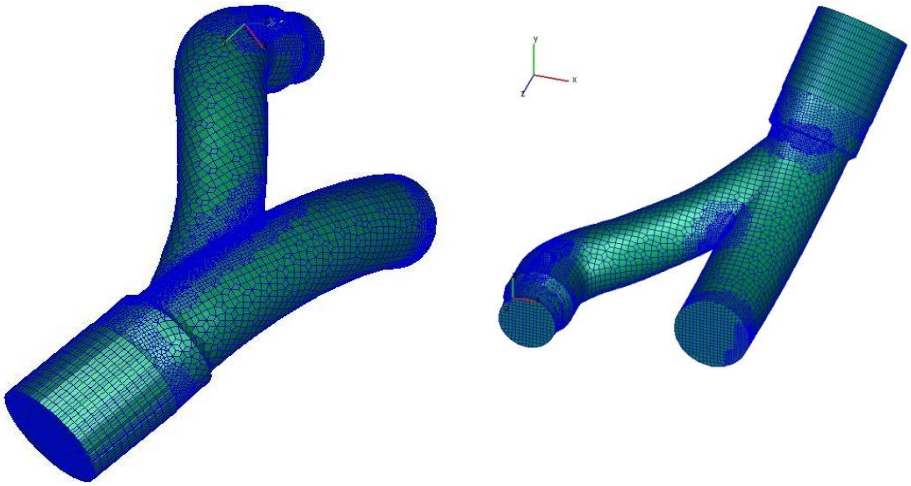

Fig. 4.3. Computing grid

4.4. The simulations of the hydrogen injection into the intake manifold

Using *AVL Fire* and CFD techniques, the distribution of hydrogen fuel in the intake manifold is determined in the simulations of hydrogen injection into the intake manifold.

Figure 4.4 specifies the boundary conditions assumed for the model: inlet air into the intake manifold, hydrogen injection, outlet pressure at the intake manifold.

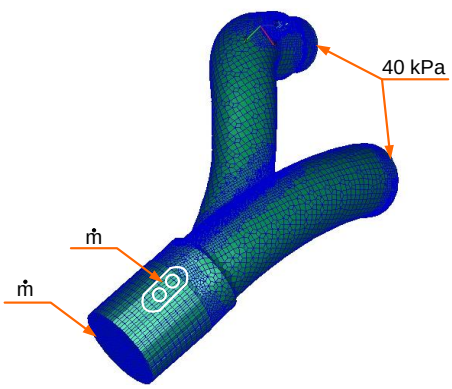

Fig. 4.4. Distribution of boundary conditions

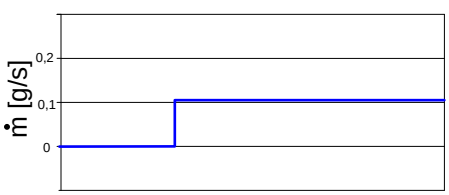

Fig. 4.5. Assumed mass flow rate of the gas injection

The inlet constant mass flow in the inlet manifold assumed amounts to 5.762 g/s. This boundary condition is defined as "Inlet". Available directly in software libraries, hydrogen is a kind of fuel used for the simulations. However, the injector models that can be used to model liquid injection available in the programme cannot be applied here directly. Therefore, to map the hydrogen injection into the manifold model at the place the injector is mounted, a boundary condition is defined as a mass flow rate (Figure 4.5). The figure below shows how the injection proceeds. The values entered into the programme are specified below. The maximum value of a mass flow rate is 0.1105 g/s. The boundary condition is defined as "Inlet". The injection is carried out with two injectors apposed, which can ensure the required mass flow through the injector and a precise dosing.

The pressure at the outlet of the intake manifold amounts to 40 kPa. This boundary condition is defined as "Outlet".

The initial conditions for a manifold model are as follows:

- pressure: 40 kPa,
- density: 1.18858 kg/m^3,
- temperature: 293.15 K,
- turbulence kinetic energy: 0.001 m^2/s^2.

Hydrogen properties:

- density: 1338 kg/m^3
- temperature: 293.15 K,
- specific heat: 12.15 kJ/K,
- thermal conductivity: 1.69 W/mK,
- enthalpy: 189.3 kJ/kg.

Assumptions for turbulent flow:

- turbulence model: k-ε,
- energy equation: active.

Timing for the simulation of the flow through the intake manifold:

- analysis type: timestep,
- analytical step: 0.05 s
- the final analysis time: 10 s,
- discretization model: second order,
- calculation module: species transport,
- frequency of results: 0.1 s.

Convergence criteria for a single step are as follow:

- maximum number of iterations for a single calculation step – 30,
- minimum number of iterations for a single calculation step – 1.

4.5. Research scope

The studies investigate how the mass flow rate through manifold intake pipes are impacted by a place of gas injector installation. Four variants of injector installation (Figure 4.6) are selected and calculated. The results are analysed for hydrogen fuel deposition and the mass flow rate through intake manifold pipes. The flow stabilises after about 350 iterations.

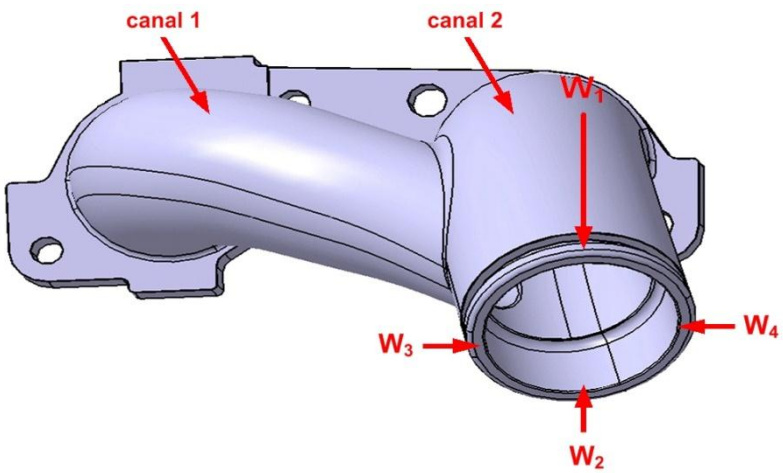

Fig. 4.6. Variants of injection nozzle installation

4.6. The simulations results

The calculations for the hydrogen injector installation are marked as W_1.

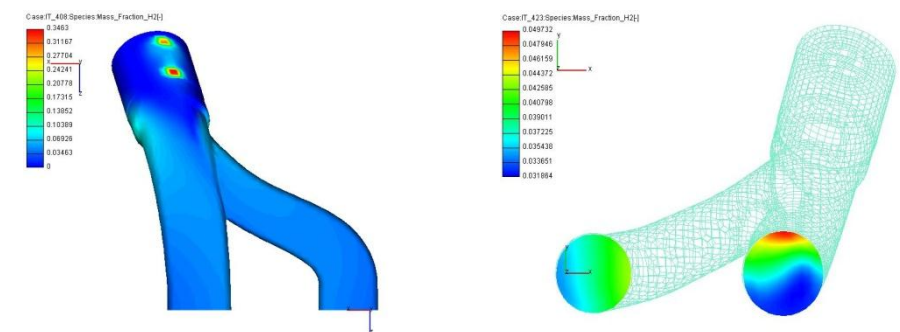

a) *b)*

Fig. 4.7. Hydrogen deposition in the intake pipe for installation option W_1:
a) on the surface, b) at the manifold outlet

The calculations for the hydrogen injector installation are marked as W_2.

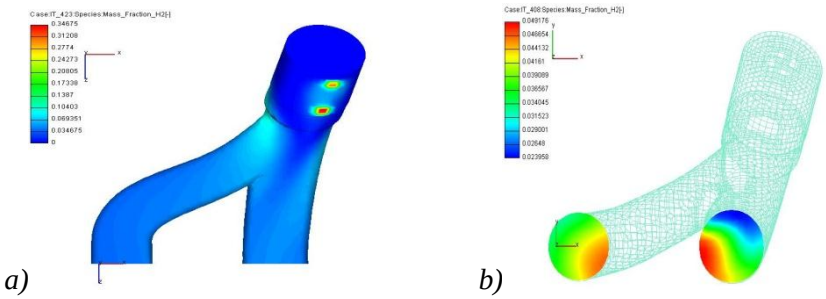

Fig. 4.8. Hydrogen deposition in the intake pipe for installation option W_2:
a) on the surface, b) at the manifold outlet

The calculations for the hydrogen injector installation are marked as W_3.

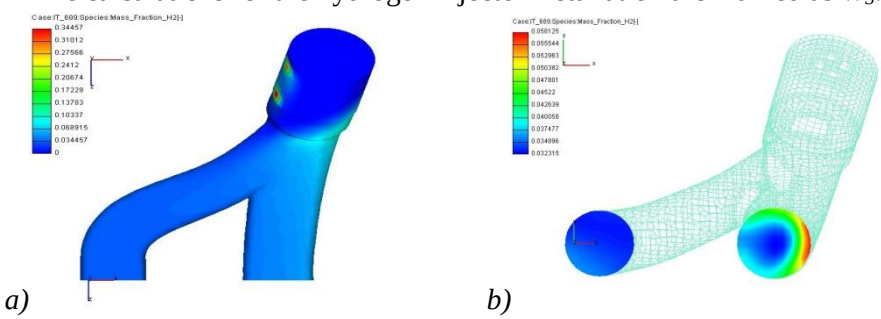

Fig. 4.9. Hydrogen deposition in the intake pipe for installation option W_3:
a) on the surface, b) at the manifold outlet

The calculations for the hydrogen injector installation are marked as W_4.

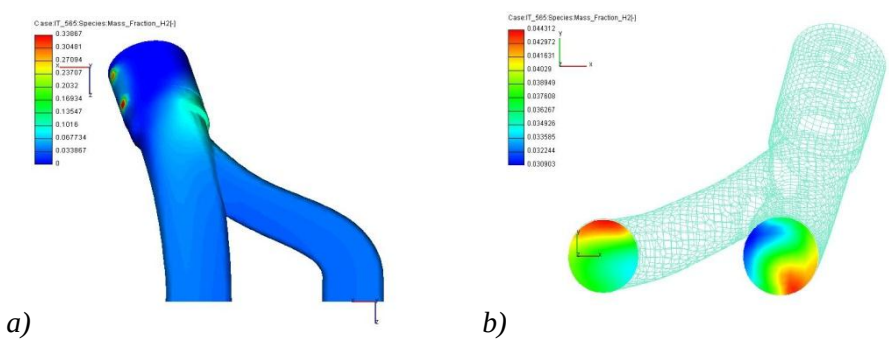

Fig. 4.10. Hydrogen deposition in the intake pipe for installation option W_4:
a) on the surface, b) at the manifold outlet

4.7. Simulation results analysis

Figures 4.11 and 4.12 show the values of the hydrogen fuel mass flow rate for four different options of injector installation. For injector installation W_1 and W_2, the values are similar in both intake pipes. For injector installation W_3, the values differ significantly so that cycle-to-cycle variation for high loads can occur. As required, fuel is correctly distributed between the intake pipes if injector installation W_4 is applied.

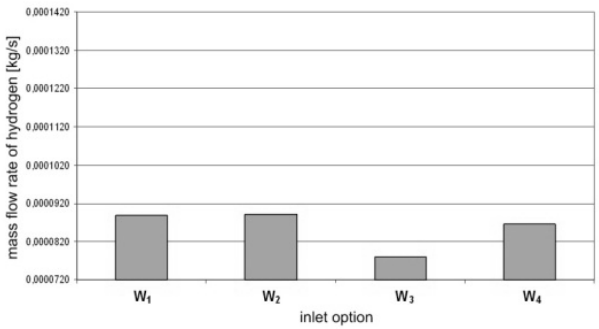

Fig. 4.11. Hydrogen mass flow rate in the intake system in pipe 1 across all the installation options

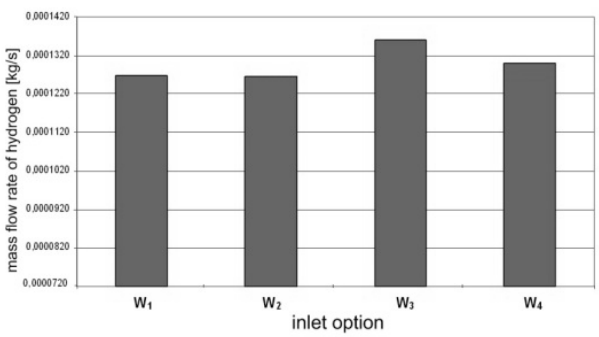

Fig. 4.12. Hydrogen mass flow rate in the intake system in pipe 2 across all the installation options

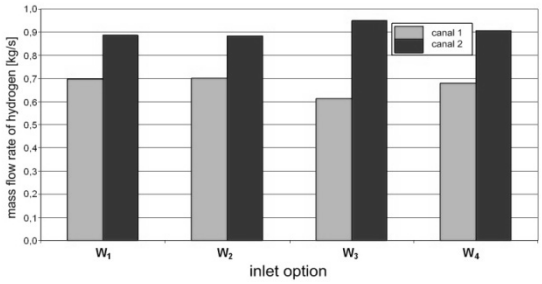

Fig. 4.13. Hydrogen mass flow rate in the intake system relative to 1 mm^2

Figure 4.13 shows the mass flow rate relative to a 1 mm^2 surface. It is noticed that the fuel is correctly distributed between the intake system ducts for injector installations W_1, W_2 and W_4. The values obtained for injector installation W_3 reduce the mass flow rate in pipe 1.

4.8. Conclusion

Each element is designed to comply with the assumptions developed in the studies to modify a hydrogen-powered Wankel engine intake system. Based on a geometry of a throttle and the injector adapter developed, injection into an intake manifold and air flow through a throttle are simulated. It can be concluded that a gas injector can be mounted as specified in W_1, W_2 or W_4.

References

[1] Ceviz M.A., Yuksel F.: *Cyclic variations on LPG and gasoline-fuelled lean burn SI engine*. Renewable Energy 31, str. 1950–1960, 2006.
[2] Jakliński P., Grabowski Ł., Wendeker M., Czarnigowski J., Szczęsny P., Barański G., Sochaczewski R.: *Analiza wpływu umieszczenia wtryskiwacza LPG na parametry pracy silnika o zapłonie iskrowym*, Silniki Spalinowe 4/2007, str. 33-41.
[3] Zervas E.: *Correlations between cycle-to-cycle variations and combustion parameters of a spark ignition engine*. Applied Thermal Engineering 24, str. 14–15, 2004.
[4] Winterbone D. E., Pearson, R. J.: *Design techniques for engine manifolds (wave action methods for IC engines)*. SAE, Warrendale, PA, USA 1999.
[5] Hernandez E.: *Simulation helps adapt intake manifold for multiple models, saving millions.* Journal articles by Fluent software users, 2002, JA174.
[6] Pogorevc P. Kegl B.*: Intake system design procedure for engines with special requirements*. 2006 220: 241 Proceedings of the Institution of Mechanical Engineers, Part D.

Michał GĘCA

5. The simulation tests of the airflow through the throttle

Abstract

The paper focuses on the airflow through the throttle in a Wankel engine (Aixro XR50). To adapt a Wankel engine to a hydrogen injection system, the author installed a new and fully electronic throttle. Consequently, an injector adapter and a flow meter are mounted on this engine. The engine is used as a stationary power unit to generate electricity for small households. Using hydrogen instead of a hydrocarbon fuel can reduce emission of greenhouse gases. The simulation is based on the AVL Fire software using Computational Fluid Dynamic for 9 different throttle opening angles, i.e. ranging from 20° to 90° (20°, 30°, 40°, 50°, 60°, 70°, 80°, 90°). The boundary conditions as the pressure at the inlet and outlet of the throttle module correspond to the real engine values. The data on the properties of the flowing medium (air) are selected by default from the AVL Fire library. The author uses a k-zeta-f turbulence model to simulate airflow in a Wankel engine throttle. The simulation results include the distributions of pressure, velocity and streamlines. The dependence of a mass flow rate as a function of a throttle position angle is discussed as well.

Keywords: airflow simulation, CFD, Wankel engine, throttle

5.1. Introduction

The simulation tests on the airflow through the Wankel engine throttle specify the dynamic phenomena inside a throttle module and a mass flow rate as a function of a throttle opening angle. These simulations precede the real modification of a Wankel engine to be hydrogen powered. The engine inlet system, which includes a throttle module, is also equipped with an injector adapter. The measurements of the electronic throttle module and the injector adapter geometry are used to develop a research model.

5.2. Geometric model for the Wankel engine throttle

This geometric model for the throttle module is made in Catia v5 and includes a throttle module throat, a throttle and an injector adapter (Fig. 5.1).

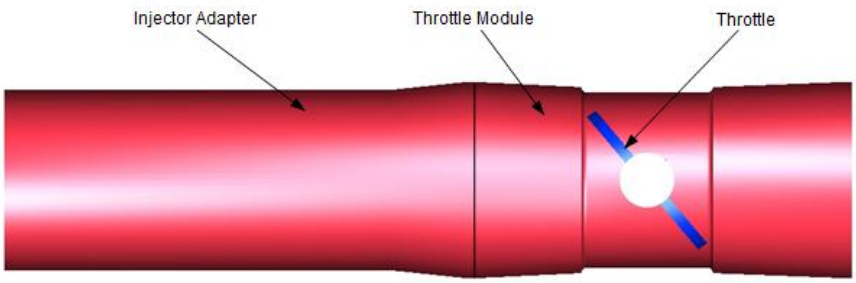

Fig. 5.1. Throttle module made in Catia v5

5.3. Boundary conditions and airflow in the throttle

The throttle airflow simulation is done for nine different throttle opening angles. As shown in Table 5.1, these angles range from 20º to 90º and correspond to a proportional range from 15.66 % to 100%.

Tab. 5.1. The angles and proportional throttle opening

model	**-**	**1**	**2**	**3**	**4**
angle	[º]	20.00	30.00	40.00	50.00
proportional opening	[%]	15.66	27.71	39.76	51.81
model	**5**	**6**	**7**	**8**	**9**
angle	60.00	70.00	75.00	80.00	90.00
proportional opening	63.86	75.90	81.93	87.95	100.00

As the geometry is complex, the number of elements in a mesh varies with a throttle position. The computing mesh adopted consists of from 150,000 to 75,000 elements (Table 5.2). To demonstrate varied computational conditions for different cases, these elements have a fixed maximum size of 2.5 mm. Basically, the mesh consists of tetrahedral elements. Figure 5.2 shows the sample mesh for one of the nine cases.

Tab. 5.2. The number of elements

model	**1**	**2**	**3**	**4**	**5**
elements	150,574	106,068	76,640	91,150	79,642
model	**6**	**7**	**8**	**9**	x
elements	80,371	78,641	79,916	75,441	x

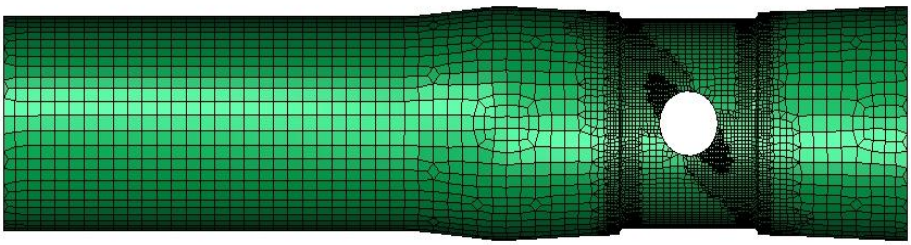

Fig. 5.2. Mesh view

The same boundary conditions and assumptions about the model are for all of the cases:

- adiabatic walls (no heat exchange with the medium),
- compressible flow,
- *k-zeta-f* turbulence model,
- the air in the model has the following properties:
  - density under NTP conditions: 1.18415 kg/m^3,
  - dynamic viscosity: 1.81 e-05 kg/ms,
  - specific heat: 1003.62 J/kg K,
  - thermal conductivity: 0.02637 W/mK,
  - molecular weight: 28.96 kg/kmol.

The simulation is under steady option, which means that the temperature and airflow do not change during the simulation. For the precise mapping of the real conditions, the boundary conditions are as follows:

- pressure at the model inlet: 100 kPa,
- inlet-outlet pressure: 99.7 kPa.

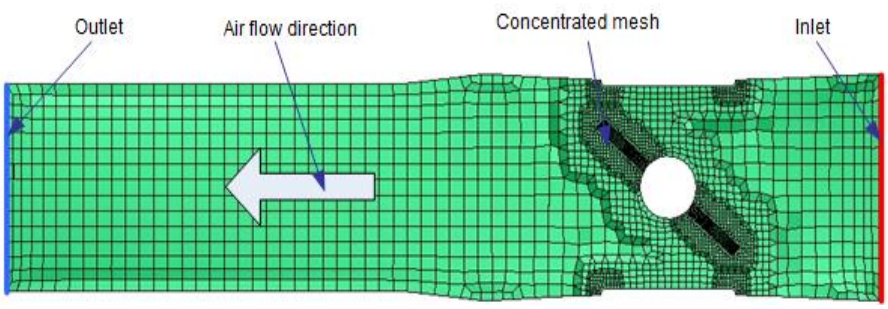

Fig. 5.3. Mesh cross-sectional view with the boundary conditions marked

All of the calculations for each model do no exceed the mass flow rate in the reference inlet. Because of different positions of the throttle, the number of iterations in the various cases ranges from 600 to 4,000. Figure 5.4 shows the mass flow rate as a function of the number of iterations (refers to a 50° throttle opening angle).

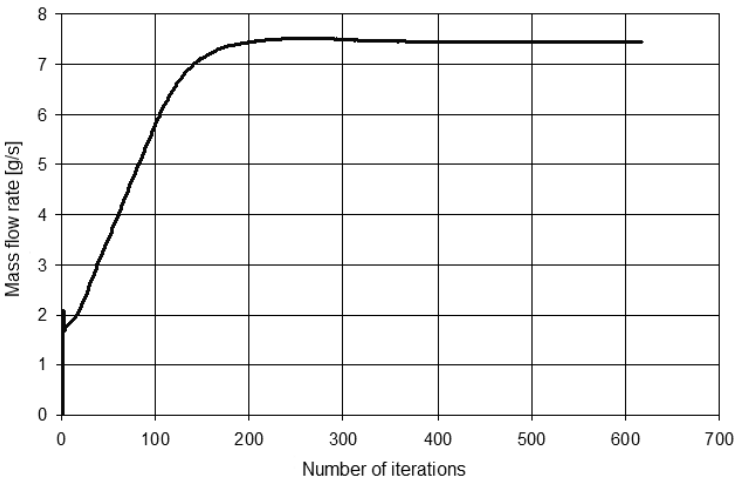

Fig. 5.4. Inlet system mass flow rate

5.4. Flow simulation results

The airflow simulation provides the distributions of pressure, velocity and streamlines in the geometric model. Figures 5.5, 5.6, 5.7, 5.8, and 5.9 present the pressure distribution in the longitudinal section for the five successive throttle positions, i.e. 20º, 40º, 60º, 80º and 90º. As noted, some significant pressure leveling at the outlet and inlet does not occur before a certain value of a throttle opening angle is obtained. This relationship is best noticed in Figures 5.6 and 5.7 that refer to opening angles of 20º and 40º. Thus, for an opening angle of 20°, the pressure at the throttle module inlet is higher than for an opening angle of 40°. For full throttle opening, i.e. 90º the pressure at the inlet throttle module remains constant until the outlet as soon as it goes through the throttle.

Figures 5.10, 5.11, 5.12, 5.13, and 5.14 present the velocity distribution for a longitudinal section for several successive throttle positions. As for the pressure distribution, the same throttle opening angles, i.e. 20º, 40º, 60º, 80º and 90º are analysed. The maximum velocity value in the throttle module is 36 m/s, which is given in Figure 5.14. It should be noted that a small change in a cross-section where this throttle is mounted, limits a higher velocity airflow area. Smaller throttle opening angles cause uneven velocity distribution, which is reflected in some turbulence in the model.

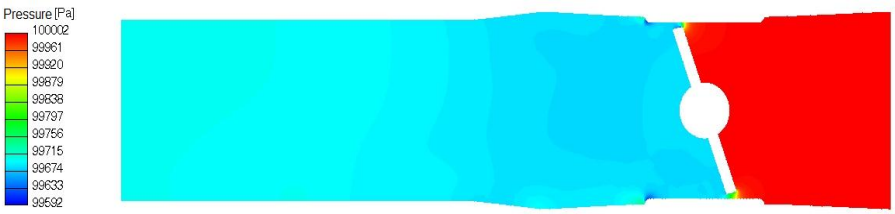

Fig. 5.5. Pressure distribution in the throttle cross-section for an angle of 20º

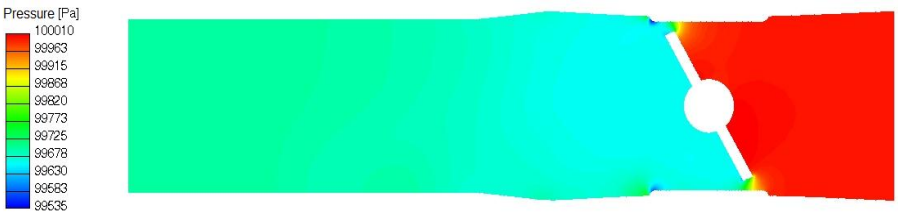

Fig. 5.6. Pressure distribution in the throttle cross-section for an angle of 40º

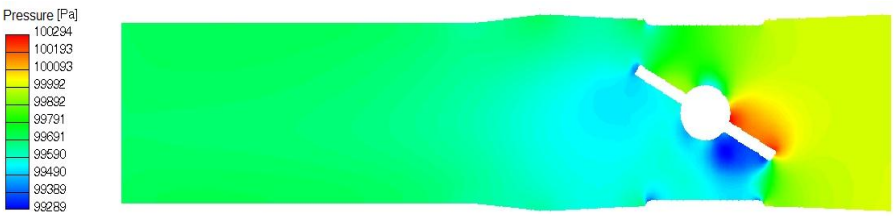

Fig. 5.7. Pressure distribution in the throttle cross-section for an angle of 60º

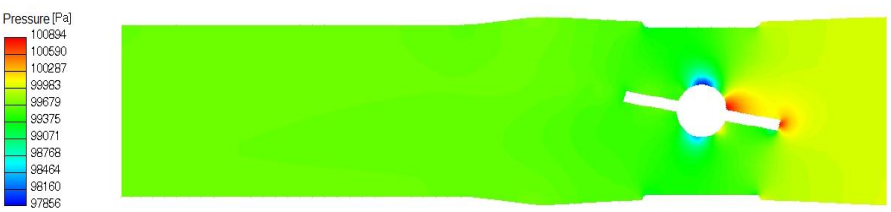

Fig. 5.8. Pressure distribution in the throttle cross-section for an angle of 80º

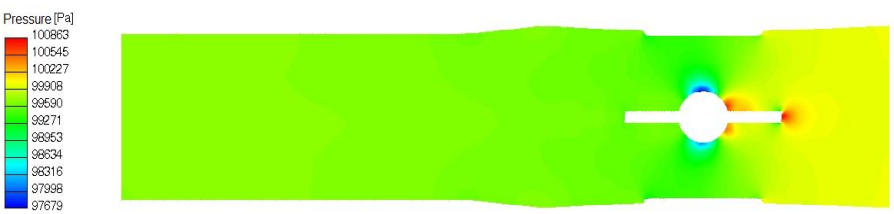

Fig. 5.9. Pressure distribution in the throttle cross-section for an angle of 90º

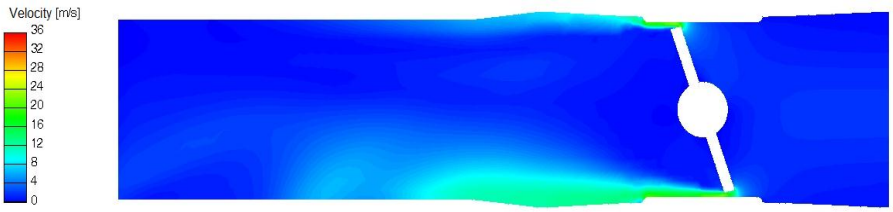

Fig. 5.10. Velocity distribution in the throttle cross-section for an angle of 20º

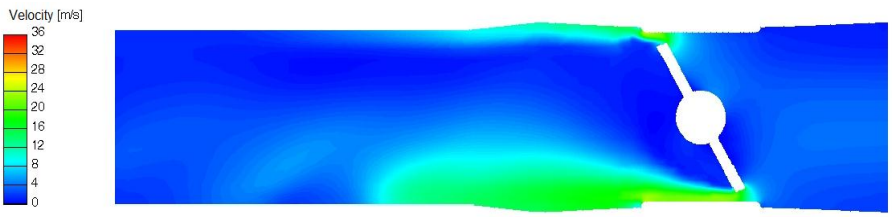

Fig. 5.11. Velocity distribution in the throttle cross-section for an angle of 40º

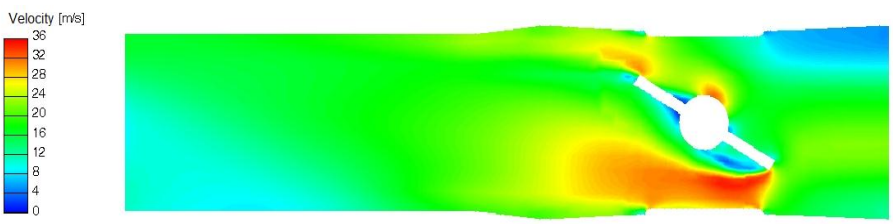

Fig. 5.12. Velocity distribution in the throttle cross-section for an angle of 60º

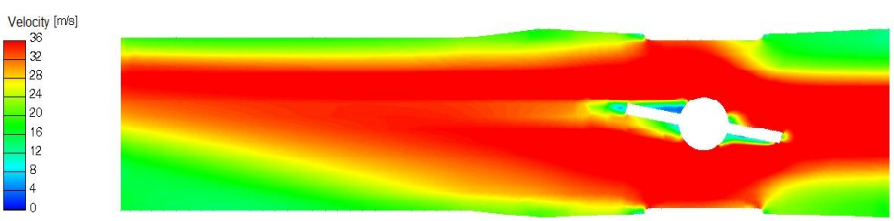

Fig. 5.13. Velocity distribution in the throttle cross-section for an angle of 80°

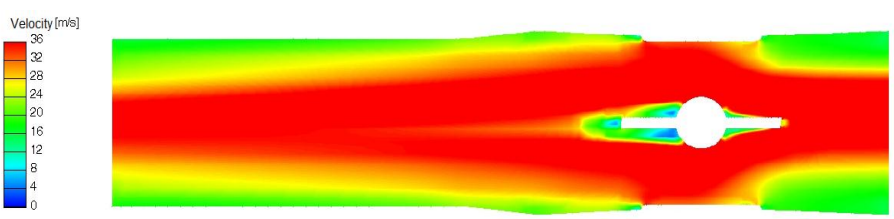

Fig. 5.14. Velocity distribution in the throttle cross-section for an angle of 90º

Figures 5.15 and 5.16 present the distribution of streamlines for a longitudinal section for the two throttle positions, i.e. 50º and 60º. The author has chosen these throttle angles on purpose because the airflow stabilises just at the change from 50º to 60º. The turbulence (see Figure 5.15) occurs for smaller throttle opening angles. This phenomenon is useful since a fuel-air mixture can be pre-mixed before it reaches the cylinder. However, if a throttle is significantly loaded and maximally opened, a lot of mixture needs to be supplied just where turbulence is not so necessary and exist no longer.

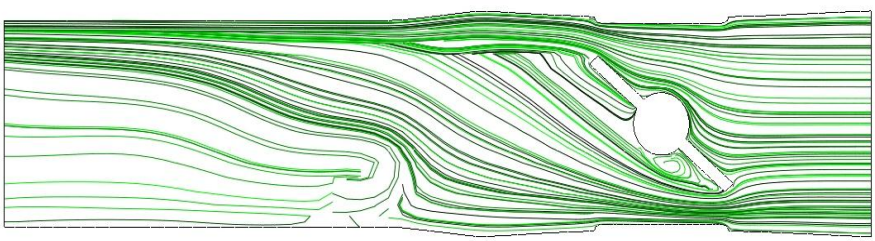

Fig. 5.15. Streamline distribution in the throttle cross-section for an angle of 50º

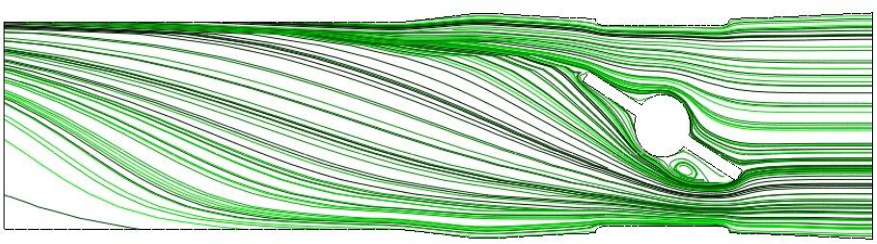

Fig. 5.16. Streamline distribution in the throttle cross-section for an angle of 60°

Based on the calculations, the relationship between the inlet pipe mass flow rate and the throttle opening angle is determined (Fig. 5.17). At a given pressure difference between the inlet and outlet, a maximum value of 24.66 g/s is obtained.

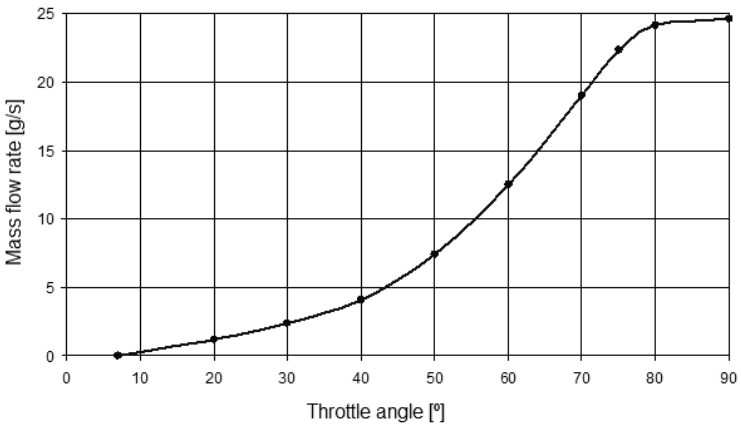

Fig. 5.17. Dependence of the mass flow rate on the angle of the throttle position

5.5. Conclusion

Based on the simulations, the maximum airflow velocity is 36 m/s. With the streamlines generated, it is found that the turbulence disappears when an throttle opening angle of 60° is crossed. Another conclusion is that for full throttle, the velocity at the pipe walls decreases to about 12 m/s. The highest velocity in the model occurs just where the throttle is mounted.

References

[1] Bogensperger, M., Ban, M., Priesching, P., Tatschl, R., *Modeling of Premixed SI-Engine Combustion Using AVL Fire – A Validation Study*, International Multidimensional Engine Modeling User's Group Meeting at the SAE Congress April 13, Detroit 2008.

[2] Puntigam, W., Uphoff, U., Fogt, H., *Numerical and experimental investigation of flow characteristics around throttle plates*, European Automotive Congress, Bratislava 2001.

[3] Tatschl, R., Basara, B., Schneider, J., Hanjalic, K., Popovac, M., Brohmer, A., Mehring, J., *Advanced Turbulent Heat Transfer Modeling for IC-Engine Applications Using AVL Fire*, International Multidimensional Engine Modeling User's Group Meeting April 2, Detroit 2006.

Rafał SOCHACZEWSKI

6. The effect of gas injection on the course of the working process of the dual-fuel diesel engine

Abstract

The paper reports the results from the simulation on how the distribution of an air-gas mixture in a diesel engine combustion chamber is impacted by an injection start angle. The research object is the 1CA90 CI engine with a single cylinder. This four-stroke engine is dual fuel, based on LPG and a diesel fuel.

A 3D model of a combustion chamber developed with AVL Fire software is studied. The air-gas mixture distribution in a combustion chamber after injecting an initiating diesel fuel dose is analysed.

The results show that changing a gaseous fuel injection start angle can significantly influence the distribution of an air-gas mixture in a diesel engine combustion chamber. Despite considerable charge turbulence, the discrepancies in gas concentration depending on injection timing are noticed. Thus, the paper specifies the values of these discrepancies and areas with a rich mixture.

Keywords: diesel engine, gas supply, gas injection start angle

6.1. Introduction

Automotive market shows an increasing tendency to use gaseous fuels to avoid high operating costs of vehicles powered by traditional fuels and to meet increasingly demanding requirements regarding CO_2 emissions.

Gaseous fuels are the most frequently used in CI internal combustion engines due to their properties similar to those of petrol vapours and an ignition system and a combustion chamber suitable for homogeneous mixtures. These fuels have got a too low cetane number and cannot initiate self-ignition. Thus, some additional energy is necessary to initiate ignition if these fuels are to power diesel engines. This is possible if an engine has got a spark ignition system [4, 7], which requires significant design changes to transform such an engine into a CI single-fuel one. Another approach involves diesel engine operation based on a dual fuel supply system, i.e. gaseous and traditional fuel [1, 2, 3, 6, 8-16] where a self-ignited small dose of diesel fuel [1, 2, 6, 8, 11 - 18] or methyl esters of fatty acid [9, 10] can initiate ignition.

The most common gaseous fuels for CI engines are: compressed natural gas (CNG) [1, 2, 14, 18], a mixture of propane and butane [1, 2, 13, 17], vapourised alcohol [6, 9, 10] or hydrogen [16].

A ratio of dosed fuels [1, 12] and ignition start, or injection timing for an initiating dose [2, 12, 15] influence the course of the combustion in a dual fuel engine. The spatial distribution of air-fuel mixture in a cylinder is another equally important parameter. Because a dual fuel engine design remains the same, certain factors that usually accompany diesel engine operation can influence mixture formation. The air supply system and the shape of the diesel engine combustion chamber are built so that turbulent flows can be achieved. Despite high air turbulence, a gaseous fuel injection angle may impact on mixture geometrical distribution.

The research on a dual fuel diesel engine powered by hydrogen and a diesel fuel described in [16] confirms that hydrogen injector opening time for an identical dose of hydrogen can influence engine operation.

This paper reports the study which has examined how the air-gas mixture formation in a dual fuel engine can be impacted by an LPG start injection.

6.2. Methodology

The modelling of the physical phenomena occurring in real objects [11, 18] is frequently analysed in the literature. A quickly developing computer technology based on engineering analyses is useful to study the issues related to medium flow. The calculation based on a one-dimensional model with the principle of mass and energy conservation in the entire modelled element is much faster but less accurate as compared to that based on CFD three-dimensional ones. Digitizing and numerical solving partial differential equations which describe the flow can determine an approximate distribution of velocity, pressure, and temperature, and other quantities to describe compressible medium flow. As a result, the author has decided to apply a CFD technology and AVL Fire which is a kind of software to model internal combustion engines.

To model the filling process in the dual fuel engine, an injection start angle α for a gaseous fuel injected into an intake duct is changed. Four successive calculation points adopted are defined by the successive angles α, i.e. -70º, 40º, 80º, and 110º (Figure 6.1) where 0° is for TDC corresponding an intake stroke start. The calculation points refer to a gaseous fuel injection into an intake duct when an intake valve is closed or open. Consequently, a gaseous fuel is injected into a medium which is at rest or in motion.

The filling process and compression for an engine operating range from -100 to 360°CA are studied. The calculations for the early angles α are done in a single calculation cycle, whereas for the late angles α in two consecutive cycles when a gaseous fuel partially remains in an intake duct. The simulation boundary and initial conditions are based on a real object bench test.

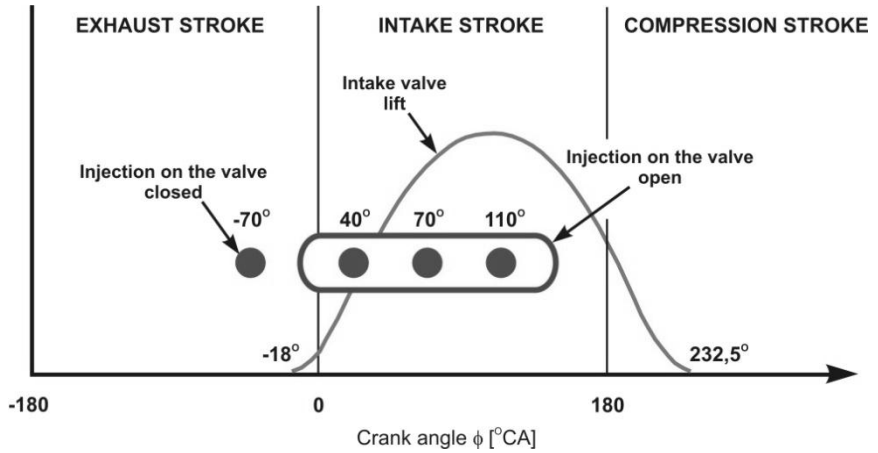

Fig. 6.1. Calculation points

The assumed values are as follows:

- engine velocity - 1800 rpm,
- inlet and outlet duct pressure - 0.1 MPa,
- gaseous fuel mass flow - 4.64 g/s.

The study assumptions are as follows:

- adiabatic walls (no heat exchange with the medium),
- compressible flow.

Air model properties:

- density under standard conditions - 1.19 kg/m^3,
- kinetic energy of turbulence - 40 m^2/s^2,
- turbulence scale - 0.028 m,
- turbulence dissipation rate - 1500 m^2/s^3,
- temperature - 293.15 K,
- k-zeta-f turbulence model.

The butane of physicochemical properties adopted from the software library is injected into the inlet duct. A gaseous fuel injection is a stroke function and lasts 1.9 ms, which assures a constant mass flow during this entire injection.

6.3. Research object

The Andoria 1CA90 internal combustion engine (Figure 6.2) is tested. This is a CI four-stroke, air cooled power unit with a single cylinder with two valves per cylinder. Its capacity, maximum power output and compression ratio are 0.573 dm^3, 6.6 kW and 16.8, respectively. Gears drive a crankshaft system. This dual fuel engine is powered by a diesel fuel injected directly into a combustion chamber and LPG injected into an intake duct.

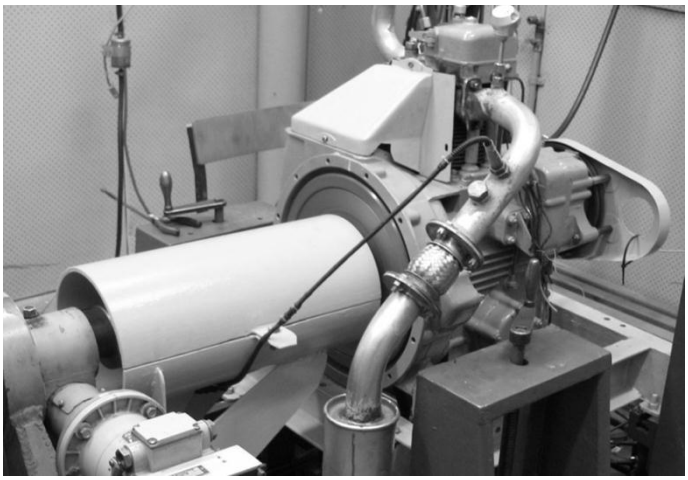

Fig. 6.2. Research object

6.4. Engine model

The cylinder and head with the inlet and outlet duct are modelled. A geometric model (Figure 6.3) made in Catia v5 is based on measurements of a real object. The model covers all the geometric elements involved in medium flow. Its whole geometry is simulated because the model is asymmetric. The model consists of the combustion chamber limited by the surfaces of the head, piston, and cylinder, the volume of the inlet and outlet duct, the external surfaces of the inlet and outlet valves, and the gaseous fuel injection nozzles.

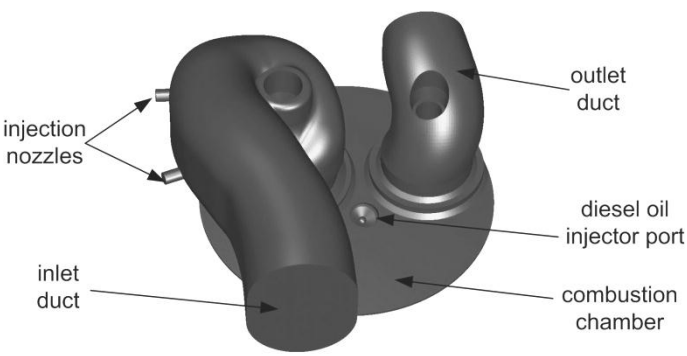

Fig. 6.3. Geometric model for the Andoria 1CA90

A digitised geometric model is used to develop this model. The computational grid consists of a minimum of 5,500 and a maximum of 205,000 cells, depending on a computational step. A cell size is generally 2.5 mm. Due to high velocity and pressure, this computational meshgrid is concentrated near the valves and faying faces so its cells are 0.3125 mm. Basically, the grid consists of tetrahedral elements, i.e. having six sides and eight vertices. Thus, this model has got a minimum of about 59,000 and up to 208,000 vertex. The model has got three moving parts, i.e. valves and piston. Figure 6.4 shows the computing grid for the engine model after discretization. The level of geometric discretization adopted provides calculation accuracy at the required level while reducing the computational time.

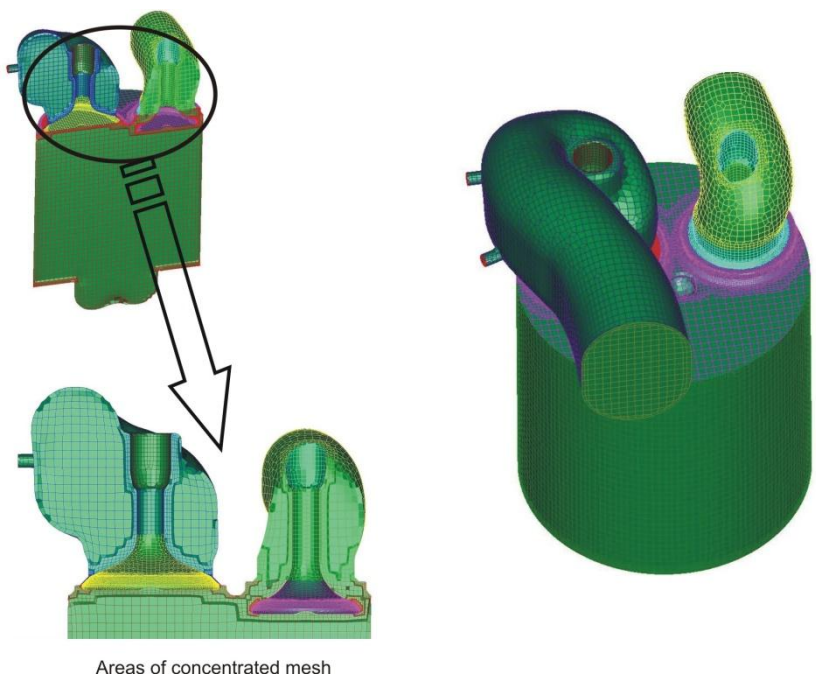

Fig. 6.4. Computing grid for the engine tested

A computational step for the simulation calculations is $\Delta\alpha$ = 1°, and 20 iterations are done. There are 5,000 iterations in each calculation point.

6.5. Simulation results

The simulation results show the gas concentration when an initiating dose of a diesel fuel is injected, i.e. 18º CA before TDC. Figure 6.5 shows the deposition of a gaseous fuel in the combustion chamber, depending on an injection start angle, i.e. in the upper and lower views of the combustion chamber and two

cross-sections of the combustion chamber through the cylinder symmetry axis, shifted relative to each other by 90°.

The simulation studies result in the courses of gas concentration changes in the inlet duct and the cylinder for selected values of α are shown on Figure 6.6.

To visualise and interpret the results correctly, a concentration scale ranging from 0.012 to 0.022 is assumed. The results allow the spatial distribution of a gaseous fuel in the cylinder to be specified.

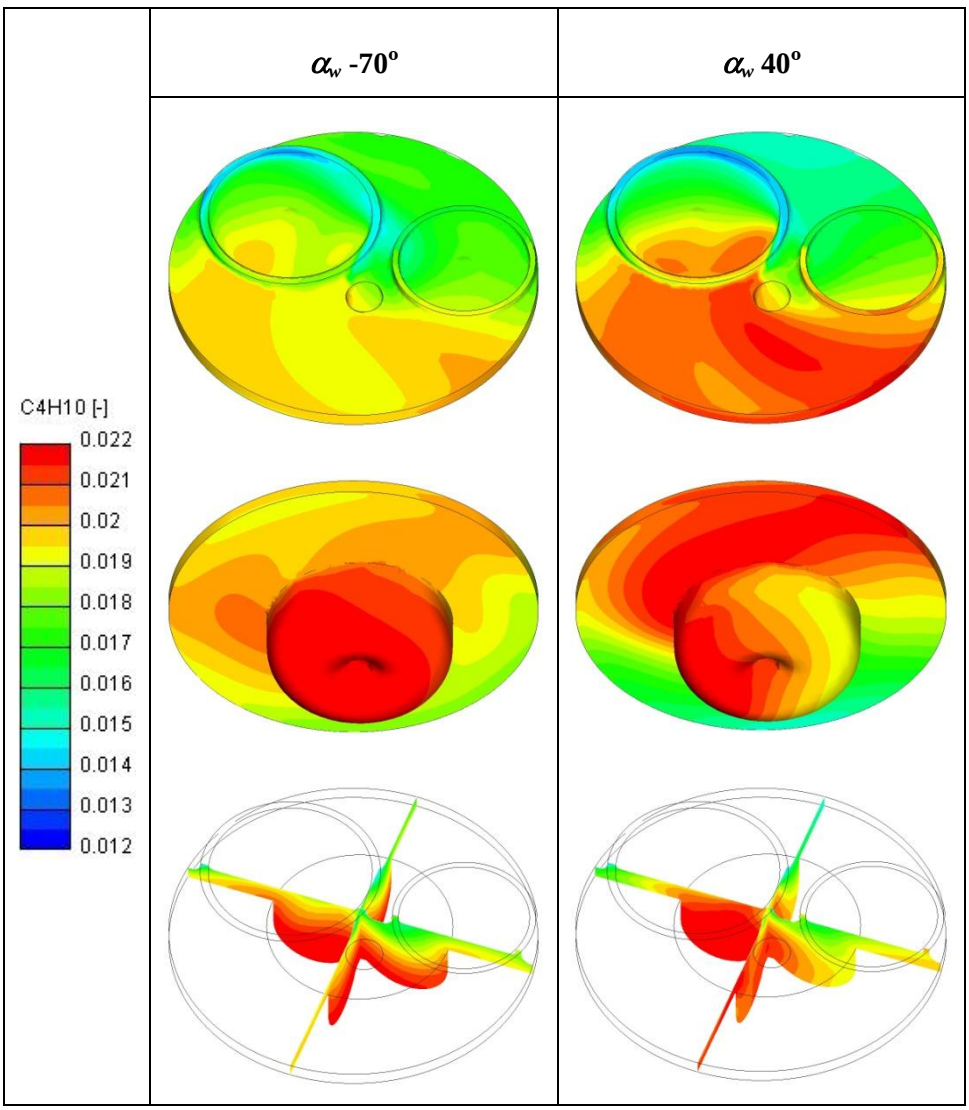

Fig. 6.5. Gaseous fuel deposition in the combustion chamber

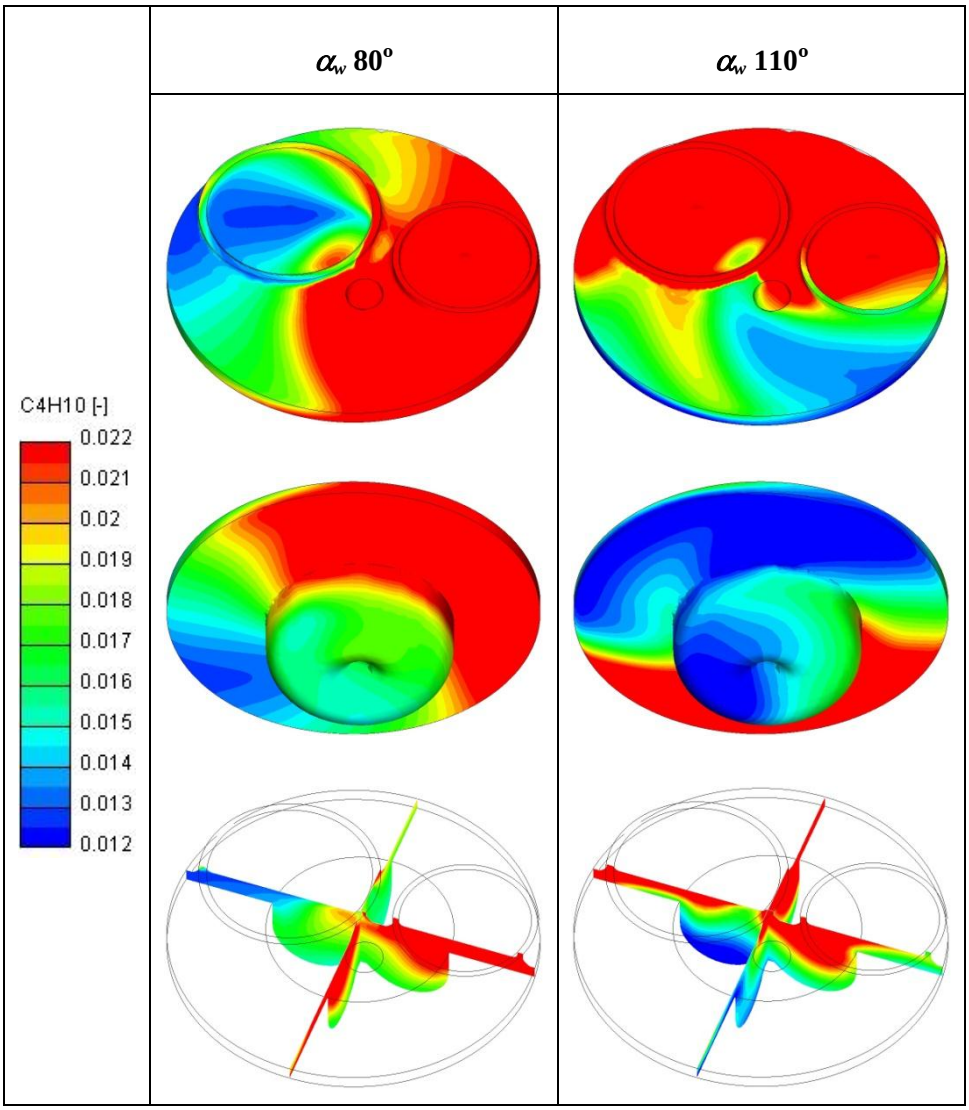

Fig. 6.5. Gaseous fuel deposition in the combustion chamber - continued

A very early injection angle start, i.e. α_w = -70º triggers air-fuel mixture formation in the intake duct (intake valve opening is 18° before TDC). Formed, a homogeneous mixture of a concentration of 0.070 flows into the cylinder when the intake valve is opened, causing a maximum instantaneous concentration of about 0.120 (see Figure 6.6). For all of the values of α_w the average gaseous fuel concentration in the cylinder is about 0.020 though discrepancies in the fuel deposition in the cylinder are notified. For α_w = -70º, a mixture of a maximum

concentration deposits at the bottom of the combustion chamber, i.e. piston crown (see Figure 6.5). As a result, the initiating dose of a diesel fuel is injected into a locally richer mixture.

A further increased injection start angle, i.e. α_w = 40° results in shifting the areas with the highest concentration from the combustion chamber into the space between the piston and head. Thus, an initiating dose is injected into the area with a leaner mixture so an increased amount of oxygen should favour the combustion of diesel fuel and then propagate a flame into the areas with a rich mixture. Later injection start angles, i.e. α_w = 80° and 110° make a minimally concentrated mixture remain at the bottom of the combustion chamber. Figure 6.5 demonstrates that the areas of a richer mixture are located between the piston and the head around the inlet and outlet valves. Such a deposited mixture may deteriorate combustion in a dual fuel engine as a result of quenching a flame in remote areas of a combustion chamber.

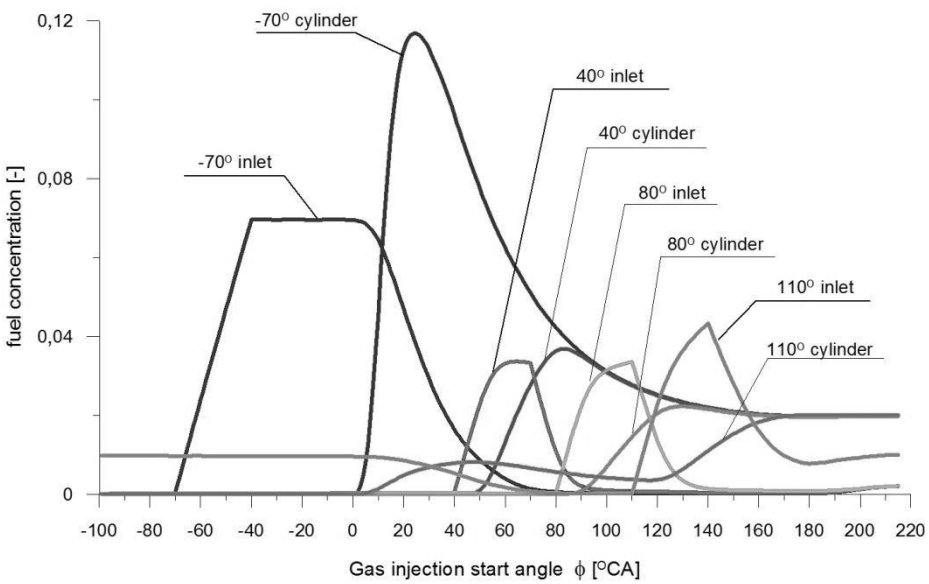

Fig. 6.6. Course of the fuel concentration in the channel inlet and the cylinder as a function of a crank angle for the characteristic changes in α_w

Later injection start angles, i.e. α_w = 40º, 80º, and 110º result in injecting a gaseous fuel into the flowing medium, which decreases the instantaneous values of the maximum concentration in the inlet duct and the cylinder. If α_w is 110°, a fuel partially remains in the inlet duct after a stroke finishes. The difference in concentration ranges from 0.010 as compared to the concentration at α_w = 70°. Consequently, the fuel mass injected in each working cycle is supplied to the combustion chamber during two cycles. Despite

a gaseous fuel is transported in two stages, its average concentration in the combustion chamber is 0.020, which means the same for all of the measurement points.

6.6. Conclusion

The diversified gaseous fuel injection in a CI dual-fuel engine has an impact on mixture formation there. The simulation results regarding the filling process show that changing an angle of a gaseous fuel start injection can significantly influence the deposition of a air-gas mixture in a combustion chamber. Despite charge turbulence is high, charge differences in the concentration of a gaseous fuel, depending on the injection timing of a fuel into the engine intake system can be noticed. Later injection start angles, i.e. α_w = 110° cause two-stage gaseous fuel transportation and the most considerable concentration differences. This contributes also to deposing this gaseous fuel in the remote areas of a combustion chamber.

A gaseous fuel injection into the medium at rest while an intake valve is closed helps homogeneous combustible mixture formation. For α_w amounted to 70°, a highly concentrated mixture is at the bottom of a combustion chamber, i.e. just where the stream of an initiating diesel fuel dose penetrates.

If this model is complemented by a combustion process and its computing grid is modified, it will be possible to determine how the medium tested can influence emissions of exhaust gases.

References

[1] Abd Alla G.H., Soliman H.A., Badr O.A., Abd Rabbo M.F.: *Effect of pilot quantity on the performance of a dual fuel engine*, Energy Conversion and Management 41, 559-572, 2000.

[2] Abd Alla G.H., Soliman H.A., Badr O.A., Abd Rabbo M.F.: *Effect of injection timing on the performance of a dual fuel engine*, Energy Conversion and Management 43, 269-277, 2002.

[3] Chan A.K.: *Ignition assist systems for direct-injected, diesel cycle, medium-duty alternative fuel engines*, Final Report Phase I, NREL/SR-540-27502, 2000

[4] Chłopek Z.: *Analiza skutków zastosowania gazu zimnego do zasilania silnika spalinowego maszyny roboczej*. SILNIKI GAZOWE wybrane zagadnienia, Częstochowa, 2010, str. 85-94.

[5] Grabowski Ł.: *Badania procesu tworzenia mieszanki w silniku o zapłonie iskrowym zasilanym wtryskiem gazu propan-butan*. Rozprawa doktorska, Politechnika Lubelska, Lublin, 2009.

[6] Kowalewicz A., Pajączek Z.: *Dual-fuel engine fuelled with ethanol and diesel fuel*, Juornal of Internal Combustion Engines KONES, Vol. 10, nr 1-2, Warszawa-Wisła, 2003.

[7] Kowalewicz A., Pawlak G., Rózycki A.: *Lean operating limit of spark ignition engine fueled with different homogeneous mixtures*, The Fourth International Symposium COMODIA 98 Proceedings, Japan, Kyoto, 1998.
[8] Kowalewicz A.: *Adaptacja silnika wysokoprężnego do zasilania gazem naturalnym*, Czasopismo Techniczne, Wydawnictwo Politechniki Krakowskiej, z. 7-M, 2008.
[9] Kowalewicz A.: *Eco-diesel engine fuelled with rapeseed oil methyl ester and ethanol*, Part 3, Combustion processes, Proc. IMechE, Part D, Journal of Automobile Engineering, Vol. 220, 1283-1291, 2006.
[10] Kowalewicz A.: *Eco-diesel engine fuelled with rapeseed oil methyl ester and ethanol*, Part 3, Efficiency and emission, Proc. IMechE, Part D, Journal of Automobile Engineering, Vol. 219, 715-723, 2005.
[11] Lee S., Kuswaka J., Daisho Y.: *Mixture Formation and Combustion Characteristics of Direcly Injected LPG Spray*. JSAE/SAE International Spring Fuels & Lubricants Meeting Yokohama, Japan, SAE 2003-01-1917, JSAE 20030009, 2003.
[12] Luft S.: *Dobór parametrów regulacyjnych dwupaliwowego silnika o zapłonie samoczynnym zasilanego głównie ciekłym gazem propan-butan*, Journal of KONES. Combustion Engines, Vol 8, No 3-4, 2001.
[13] Luft S.: *Dwupaliwowy silnik o zapłonie samoczynnym z wtryskiem ciekłego LPG do kolektora dolotowego*, Wyd. Politechniki Radomskiej, Radom, 2007.
[14] Papagiannakis R.G., Hounatalas D.T.: *Combustion and exhaust emission characteristics of a dual fuel compression ignition engine operated with pilot Diesel fuel and natural gas*, Energy Conversion and Management 45 (2004) 2971-2987.
[15] Ramadhas A. S., Jayaraj S., Muraleedharan C.: *Performance and emission studies on biodiesel-liquefied petroleum gas dual fuel engine with exhaust gas recirculation*. Journal of Renewable and Sustainable Energy 2, 013109, 2010.
[16] Saravanan N., Nagarajan G., Dhanasekaran C., Kalaiselvan M.: *Expermental investigation of hydrogen fuel injection in DI dual fuel diesel engine*, SAE Paper 2007-01-1465, 2007.
[17] Sochaczewski R., Wendeker M., Czarnigowski J., Jakliński P., Barański G., Poleszak J., Zyska T.: *Dual fuel diesel engine examinations*, Kongres Silników Spalinowych 2007 PTNSS, P07-C155, Silniki Spalinowe PTNSS-2007-SC1, str. 186-192.
[18] Stelmasiak Z.: *Studium procesu spalania w dwupaliwowym silniku o zapłonie samoczynnym zasilanym gazem ziemnym i olejem napędowym*, Wydawnictwo Akademii Techniczno-Humanistycznej w Bielsku-Białej, Bielsko Biała, 2003.

Adam MAJCZAK, Paweł MAGRYTA

7. The effect of design parameters on the process of gas supply in the spark ignition engine

Abstract

The paper presents how the filling process in a propane-butane fuelled engine is modelled. The modelling of a geometry employs a real 4-cylinder SI engine with a 2 dm^3 displacement. The AVL Fire software is used for engine modelling and simulations. Fuel mass supplied to a cylinder is identical for all of the cases. The study is performed for several injector opening times and some values of injection mass flow rate. The study examines how the fuel deposition in a combustion chamber is impacted by an gas mass flow rate in an injector. A change in an injection course is demonstrated to influence fuel distribution in a cylinder. Also, fuel concentration near a spark plug is specified.

Keywords: combustion engine, gas injection, modelling, CFD

7.1. Introduction

According to the statistics, the number of cars with LPG supplied engines has been steadily increasing in Poland for several years [7]. As a result, Poland is at the forefront of LPG consumption for engine applications among European countries.

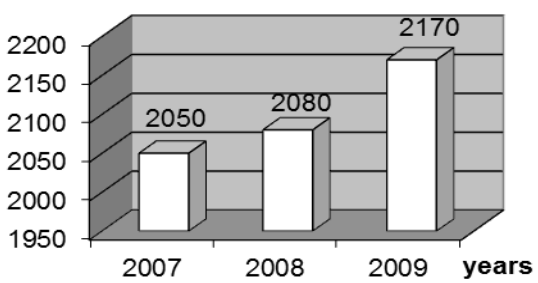

Fig. 7.1. LPG fuelled vehicles (in thousands) in Poland [7]

This strong interest in LPG is due to its relatively low price in relation to petrol and the possibility of improving engine performance by enhanced supplying systems.

Currently, LPG sequential gas injection systems, i.e. fourth generation systems are the most common ones. No changes in a gas engine design are

required, if this system is mounted in a vehicle. As LPG is condensed at a 6 bar its storage and transportation are safe.

LPG supply systems are based on injecting vapourised LPG into engine inlet pipes (as in multi-point petrol injection systems). LPG injection is done by joined electromagnetic injectors to form a fuel injection unit. Injected gas flows along pipes into injection nozzles mounted at an intake pipe. This approach is adopted due to the difficulty in mounting separate gas injectors in modern vehicles, which is related to hardly accessible inlet pipes. Injection pipes depending on a vehicle are mounted in different configurations of diameter and length, which can influence injection. The impact of this factor can be reduced by adjusting fuel injection timing and flow [3], [2], [4].

The phenomena that accompany gas injection were analysed to eliminate any adverse phenomena during gas flow. This complex issue and the comprehensive analysis of processes while the engine is filled contribute to carrying out CFD simulation to explain the relations noticed. The use of numerical fluid dynamics to study the process of filling the gas-fuelled engine is discussed in [1], [5], [6]. The process of filling a cylinder with an air-fuel mixture depends on a geometry of a system that doses a gas, i.e. injection pipe diameter and length, injection nozzle diameter, and a distance between an injection nozzle and an axis of an intake valve. This paper discusses the research results on how the timing of gas injection into an inlet manifold can influence the fuel deposition in a combustion chamber.

7.2. Research methodology

CFD calculations based on the *AVL Fire* software can specify how an engine filling is influenced by an LPG mass flow rate through an injector. The same software is used to develop a model by digitizing the geometry developed in CATIA v5. About 230,000 computational cells are obtained (Fig. 7.2).

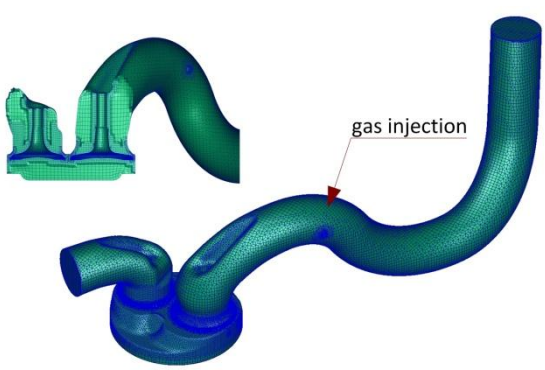

Fig. 7.2. Computational grid

A 4-cylinder SI engine with a displacement of 2000 cm^3 is a reference model for this computational geometric model. Based on the tests on a real object, the initial boundary conditions for simulations are as follows:

- rotational speed – 1,900 rpm,
- inlet pressure – 60 kPa,
- outlet pressure – 100 kPa,
- initial pressure in the inlet pipe – 60 kPa,
- initial pressure in the outlet pipe and cylinder – 60 kPa.

The assumptions for the study include:

- adiabatic walls (no heat exchange with a medium),
- compressible flow.

Air model properties are:

- ρ under normal conditions – 1.1841 kg/m^3,
- dynamic viscosity – 1.81 e-05kg/ms,
- specific heat – 1,003.62 J/kg K,
- thermal conductivity – 0.02637 W/mK,
- molecular weight – 28.96 kg/kmol,
- *k-zeta-f* turbulence model.

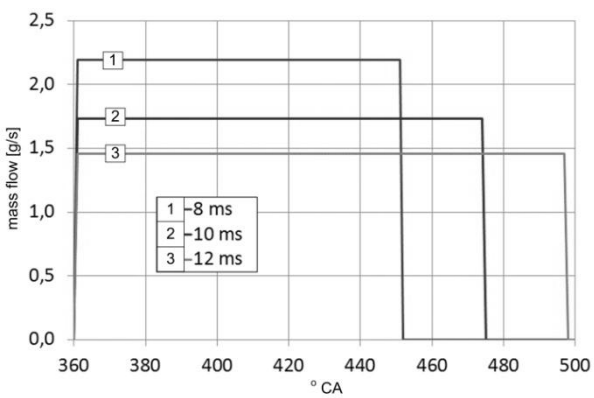

Fig. 7.3. Fuel injection for different injection times

Propane is injected into the intake manifold. The calculations are done for three injection timings for the gas mass flow through the injection nozzle (Fig. 7.3), i.e. 8 ms, 10 ms, and 12 ms. The same fuel mass supplied to the intake pipe is recorded for all the timings. Given the objective of the modelling, the calculations refer to a filling process only, and the simulations finish at ignition, i.e. 20° before TDC. The fuel deposition and concentration in the combustion chamber are analysed.

7.3. Research results

The simulations specify the courses of the fuel mass changes in the intake pipe and the cylinder for all the types of injection (Fig. 7.4). For the initial injection phase, i.e. 360 – 400° CA an increase in fuel mass in the intake is linear. This is due to a backflow of exhaust gases from the exhaust pipe and the cylinder to the intake pipe. This phenomenon is caused by a pressure difference for partial engine load (60 kPa). Figure 7.5 shows the flow move directly from the outlet pipe to the inlet one.

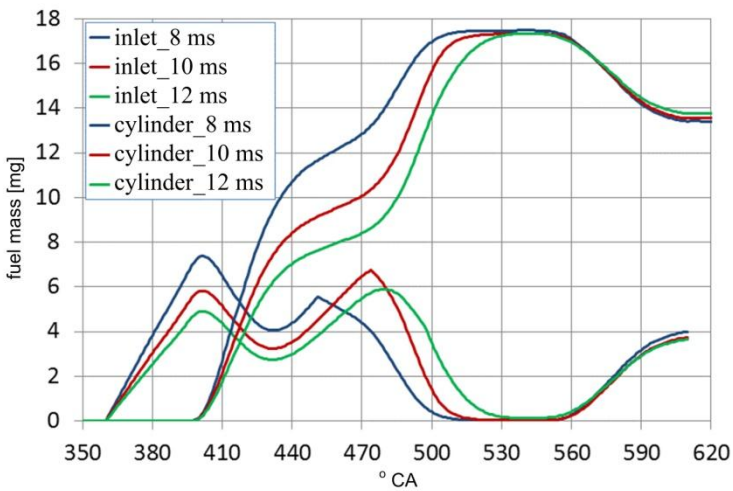

Fig. 7.4. Fuel mass in the inlet pipe and the cylinder

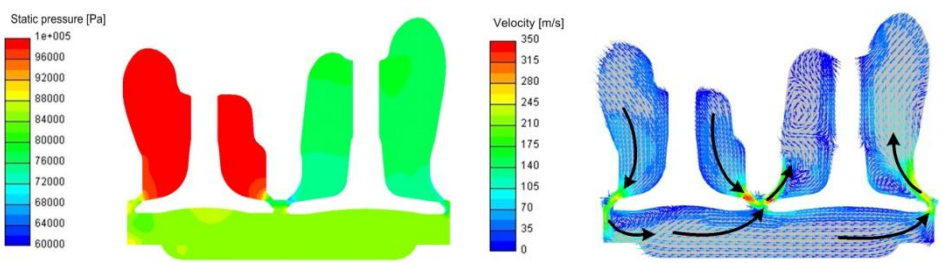

Fig. 7.5. Static pressure and velocity distribution at 360° CA

Figure 7.6 shows the fuel distribution in the intake pipe when a flow direction changes (390° CA), which is due to closing the intake valve (395° CA) and levelling the pressure in the cylinder and the intake pipe. Depending on the type of injection,the fuel goes back towards the inlet for a different distance.

This distance increases as injection time decreases (higher injection intensity). However, the fuel outflows through the inlet section in none of the cases because the intake pipe is long enough to prevent this at such an inlet pressure. For lower loads, the fuel may escape to the manifold, which may result in the non-uniform supplying of individual cylinders [2].

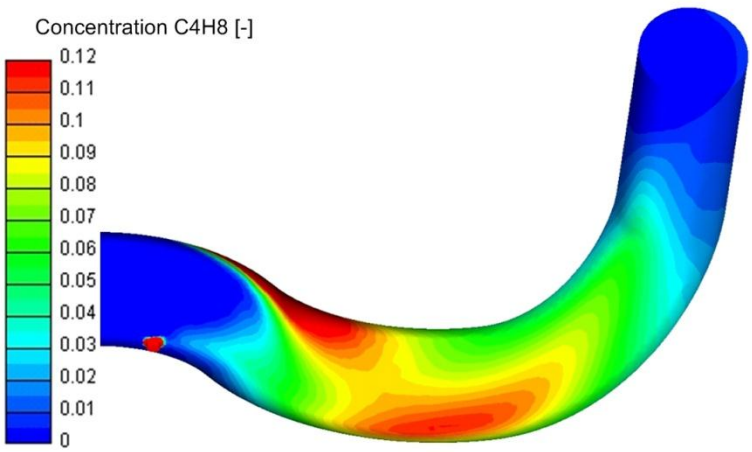

Fig. 7.6. Fuel distribution in the inlet pipe at 390° CA

An increase in fuel mass in the cylinder starts for 390° CA; and the highest mass flow is for a time of 8 ms. This is due to the largest fuel mass accumulated in the intake pipe. Fuel transportation into the cylinder ends as late as a time of 12 ms (about 545° CA). Then, the fuel starts flowing out of the cylinder, which is due to a backflow caused by decreasing cylinder volume; and the intake valve remains open (Fig. 7.7).

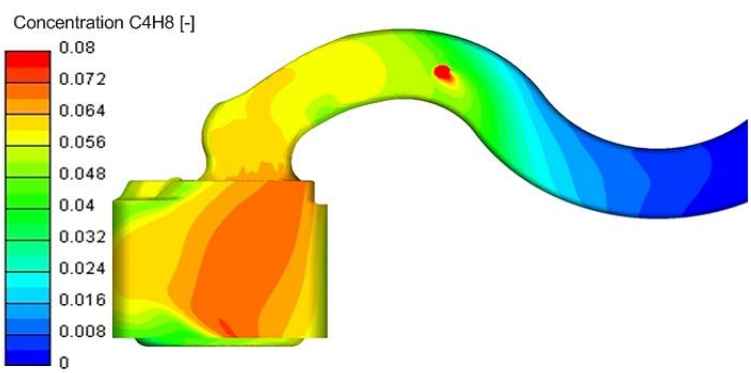

Fig. 7.7. Fuel distribution in the inlet pipe at 610° CA

For injection time longer than 12 ms, the fuel injected would not get into the cylinder. The fuel mass in the cylinder is reduced from 17.3 to 13.8 mg, or by about 20%. This fuel remains in the intake pipe until the next engine cycle. The backflow makes the mixture in the cylinder leaner. However, the composition of the mixture should be set at a constant reference level in subsequent cycles.

The average fuel concentration in the cylinder for all the cases is set in around 0.054. Figure 7.7 shows that the fuel distribution in the cylinder at ignition (700° CA) varies considerably depending on injection time. Differences are noticed for both maximum concentration and geometric location of an area with the richest mixture. The mixture is the most homogenous for the longest injection time (Fig. 7.8) because more time is needed to mix propane and air. For the shortest injection time, the highest maximum concentration is recorded, which results from a rich mixture area, formed already during injection. Even at the end of the compression stroke, this area is clearly visible in the combustion chamber (Fig. 7.7).

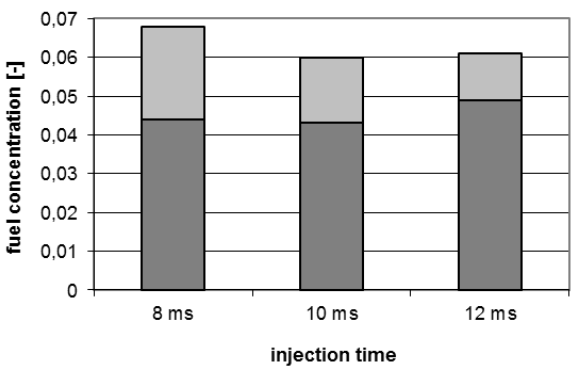

Fig. 7.8. Fuel concentration in the cylinder (700° CA)

The location of a rich mixture area at ignition varies considerably depending on injection (Fig. 7.9). For an injection time of 8 ms, the richest mixture accumulates around the spark plug and the highest maximum concentration is noticed, which is beneficial for ignition. For an injection time of 12 ms, the maximum concentration is around the intake valve seat. For an injection time of 10 ms, it is between the inlet valve and the spark plug.

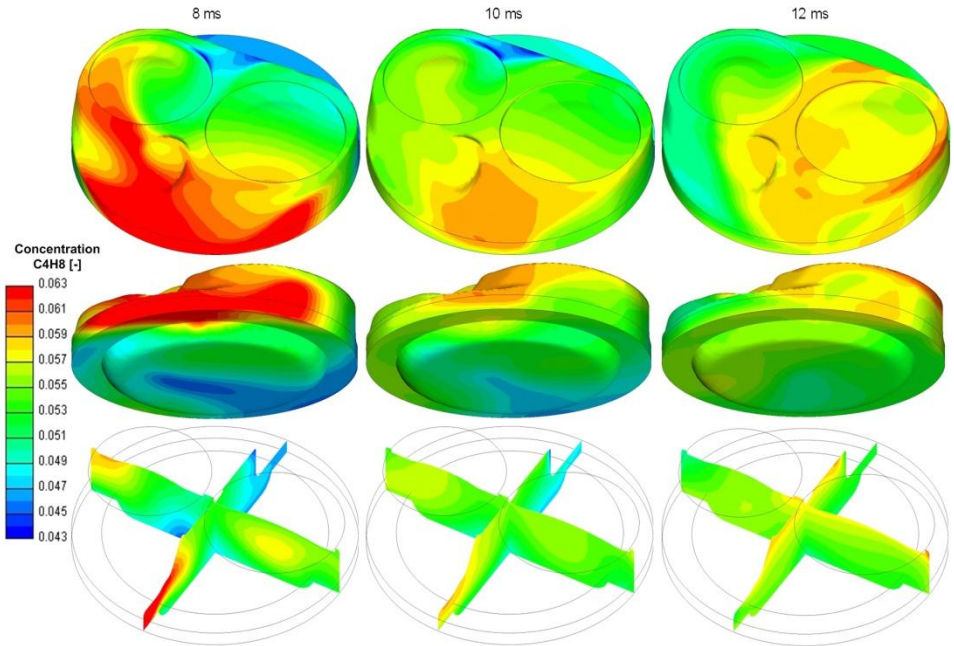

Fig. 7.9. Fuel distribution in the combustion chamber at 700° CA

7.4. Conclusion

At a partial loading of 60 kPa, a significant backflow through the inlet valve is noted at the end of the exhaust stroke. Consequently, the fuel injected moves backwards the inlet of the intake pipe. No fuel, however, flows outside.

The entire mass of the gas injected is sucked during a cylinder filling. However, the backflow that precedes closing the intake valve pushes out some fuel mixed with air into the intake pipe. Thus, such a mixture is leaner and will be sucked into the cylinder in the next filling cycle. The mixture composition will be then at the reference value.

The mean fuel concentration in the combustion chamber at ignition is the same for all the cases. However, the fuel distribution and fuel mixing are different. Mixture stratification increases as injection time decreases. The best conditions for ignition, i.e. high fuel concentration near the spark plug are for the shortest injection time.

Further studies will examine more precisely the impact of injection timing on fuel distribution in a cylinder. Thus, this modelling needs to be supplemented with a combustion process, and the computational grid needs to be modified to calculate the next operating cycle.

References

[1] Bahram K., Haworth D., Hubler.: *Multidimensional Port and In-Cylinder visualization Flow Calculations and Flow Vision Study in an Internal Combustion Engine with Different Intake Configurations*. SAE Technical Paper nr 941871, 1994.
[2] Grabowski Ł., Wendeker M.: *The Mixture Formation Process In The Gas Fuelled Engine*. Monografia, Wydawnictwo Politechniki Lubelskiej, 2010.
[3] Jakliński P., Czarnigowski J., Wendeker M.: *The effect of injection start angle of vaporized LPG on SI engine operation parameters*. SAE Technical Paper nr 2007-01-2054, 2007.
[4] Lee Y., Kim Ch., OH S Kang K.: *Effets of Injection Timing on Mixture Distribution in a Liquid-Phase LPG Injection Engine for a heavy-DutyVehicle*. Vol. 47 (2004), No. 2 Special Issue on International Conferences on Power and Energy System pp. 410-415.
[5] Semin, Ismail A. R., Bakar R. A.: *Smiulation Investigation of Intake Static Pressure of CNG Engine*, Journal of Engineering and Applied Sciences 3 (9): p. 718-724, Medwell Journals, 2008.
[6] Shashikantha E., Parikh P. P.: *Spark ignition producer gas engine and dedicated compressed natural gas engine – technology development and experimental performance optimization*. SAE Technical Paper nr 1999-01-3515, 1999.
[7] http://www.motofakty.pl.

Marcin SZLACHETKA, Michał BIAŁY

8. The modelling of the external characteristics of the Wankel engine

Abstract

This paper describes the Wankel engine model developed with the AVL BOOST programme which is a multi-level system for a real-time processing and simulating variable engine operating conditions. The standard modules available in the system are used for this research. The tested object is a low intake, 4-stroke XR50 Wankel engine. The torque-speed characteristics is determined. The model is calibrated by comparing the torque calculated to the experimental external engine characteristics. The error for the torque calculated does not exceed 6 % for most measurement points. In fact, no satisfactory conformity has been achieved for the highest speeds only. This Wankel engine model will be used later to model this type of engine for hydrogen injection.

Keywords: Wankel engine, phenomenological model, simulation

8.1. Introduction

Physical modelling is widely reported in the automotive literature [1, 6, 9]. The advantage of a zero-dimensional model over three-dimensional ones is short computation time. The former method employs the principle of mass and energy conservation in the entire element modelled (e.g. an intake pipe or a cylinder).

The mapping of the processes that occur in a combustion engine enables analysing crank system dynamics and specifying critical parameters for a medium in a cylinder for defined operating conditions [4, 7, 8]. The engine model developed in a Modelica simulation environment is discussed in the paper in [2]. The detailed characteristics of its design includes listing all the phenomena where mathematical mapping is necessary for accurate modelling an engine. The authors claim that modelling is an indispensable task to design both an engine and fuelling systems.

A simulation software can be used for research as it is discussed in the paper in [10]. The researchers developed a model of a single-cylinder SI engine, and their results have enabled a preliminary analysis of engine performance.

In the literature, the modelling of Wankel engine operation is discussed in few papers. Research done by companies like AVL and FEV confirm that this type of engine is popular [3,11]. These companies independently of each other have developed a Wankel-engine-powered generator to charge batteries. Based

on his tests, Izweik H. T. in his doctoral dissertation [5] claimed that a Wankel engine design is very suitable for using gaseous fuels.

This paper discusses a zero-dimensional model of such an engine developed in AVL BOOST. As no model for a Wankel engine working space is available in the software libraries, the components available are used for modelling. The engine operation analysis enables mapping the engine working process with a typical piston system.

8.2. AVL BOOST

The AVL BOOST software is a multi-module system which can work in real time. It is dedicated to simulate variable conditions of engine operation. The software is a package to simulate engine operation in a time domain, using temporary and permanent zero-dimensional and quasi-dimensional model components.

AVL BOOST contains dedicated, core engine components to ensure flexibility in engine modelling. These components fall into five main groups to deal with:

- liquid and gas properties, an inlet manifold, an air filter, a cylinder, a compressor, a fuel tank, fuel film, a turbine,
- a thermal environment: heat transfer with an environment,
- a mechanical environment: drive system inertia, vehicle movement resistance,
- a control environment: injection characteristics, a PID controller,
- interfaces: C-interface, Matlab DLL, Matlab API.

Each component contains relevant computational models. The components which describe a gas stream and thermal and mechanical environments include models to simulate:

- flow with gas properties and corresponding equilibrium equations,
- heat transfer in a combustion chamber and pipes,
- a combustion process,
- fuel injection,
- friction in an engine,
- fuel film,
- injection mapping and characteristics for valve lifts,
- turbines of varied geometries,
- mechanical compressors,
- flow through an air filter,
- heat exchangers.

AVL BOOST interface can be used to start modelling as connected to other system tools such as AVL Fire and AVL CRUISE.

8.3. Research object

The modelling is done for the XR50 intake flow 4-stroke Wankel engine by Aixro GmbH. Its parameters are specified in Table 8.1.

The engine is based on Felix Wankel's patent. The key components include:

- a sealed steel rotor (analogous to a piston with rings in a piston engine),
- a steel eccentric shaft,
- an epitrochoidal aluminum body with its nickel plated inner surface,
- aluminum side covers.

Tab. 8.1. XR50 engine specification

parameter	value and unit
power	33 kW at 8,750 rpm
torque	39 Nm at 7,500 rpm
weight	17 kg
chamber volume	294 cm^3
max. rpm	10,400 rpm
ignition	magneto
clutch	dry centrifigural
drive	½ chain type 428
spark plug	Denso U22ETR
starter	12 V / 0.4 kW

The rotor edges remain in permanent contact with the epitrochoid thanks to the sealed peaks. Thus, they form three separate combustion chambers out of each rotor surface, which allows three cycles at the same time. The rotor rotates three times slower than the eccentric shaft, and ignition occurs in a combustion chamber during each shaft rotation.

In-mixture lubrication is applied in the XR50 engine. An air-fuel mixture flows into the combustion chamber through the rotor interior and cools and lubricates the eccentric shaft bearings. For speeds higher than 5,500 rpm, the throttle in the second channel of the intake pipe opens. Additional air-fuel mixture flow is controlled by the under pressure valve which is connected to the nozzle in the carburetor (blue line in Figure 8.2). The air-fuel mixture which does not cool the bearings and the rotor is provided directly to the combustion chamber. This increases engine filling efficiency.

Figure 8.2 shows the fuel system in the XR50 engine. The fuel path is marked orange. The fuel pump sucks fuel from the tank to the YSN PWK30 carburetor through a membrane filter. The vent pipes are marked black.

Fig. 8.1. Research object

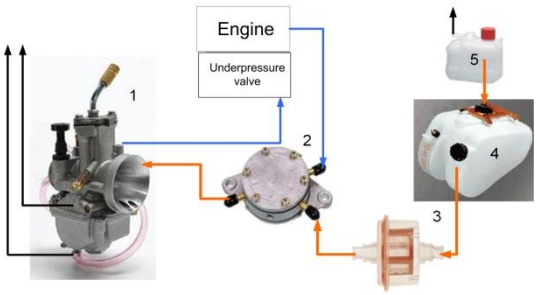

Fig. 8.2. Scheme of the fuel system in Aixro XR50, 1 – carburettor, 2 – fuel pump, 3 – fuel filter, 4 – fuel tank, 5 – expansion tank

8.4. XR50 engine model

The AVL BOOST software to simulate combustion engine operation has been used to model the XR50 engine. Figure 8.3 shows the models of the engine components.

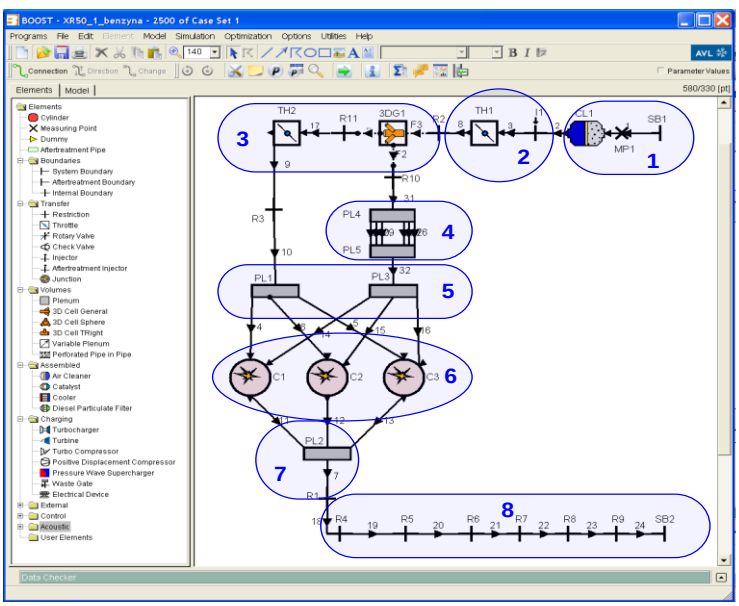

Fig. 8.3. Engine model in AVL BOOST software, 1 – air inlet, 2 – carburettor, 3 – air-fuel mixture line separation, 4 – rotor, 5 – inlet pipes in the engine body, 6 – engine workspace, 7 – outlet pipes in the engine body, 8 – exhaust system

The model for the medium flow in the inlet and outlet system is generally simplified by replacing complex-shaped pipes with those of a round section. If necessary, pipes of a variable diameter, i.e. cone-shaped and pipes of a curvilinear axis, i.e. arcs of a specified radius are used. The Wankel engine carburetor is modelled using a cable connected to the injector supplying fuel continuously. An injector flow rate depends on a mass flow rate and is selected automatically to maintain stoichiometric mixture composition.

The standard components available in the software are used to model the engine (Figure 8.3, left side in the window). Thus, it is necessary to simplify the structure components as shown in Table 8.2.

Tab. 8.2. Functions for modelling

function	symbol	quantity
system boundary	SB	2
restriction	R	14
injector	I	1
measurment point	MP	3
air cleaner	AC	1
cylinder	C	3
plenum	P	4
connection	-	29

The engine working space is the most simplified element in the model. The Wankel engine volume is changed by the rotor moving in a specially shaped epitrochoidal area. The working space is modelled using three Cylinder elements in BOOST. This simplification is necessary due to the fact that this software has got no special element to model a Wankel engine. It is assumed that the shape of the combustion chamber is irrelevant due to the model is zero-dimensional. Therefore, a Wankel engine model can be replaced by a 3-cylinder piston engine model.

The connections of the working spaces (C1, C2, C3) with the inlet pipes (12, 29) and the outlet channel (8) are also simplified. The charge reaches the cylinders through the channels inside the engine head (individual channels for each cylinder); whereas the working spaces in the Wankel engine rotor share the common channels inside the engine body. As a result, it is necessary to use so called *Plenum* components of small volume (0.005 dm^3) in the model and connect them to the working spaces with 3 mm pipes. This simplification can ensure continuous medium flow in the main inlet and outlet channel.

A Wankel engine operation cycle is the same as in a 4-stroke engine. It has got identical phases like filling, compression, decompression, and outlet. The volume of the working space varies sinusoidally, which is ensured by a connecting rod of 1,000 mm and a bore of 180.5 mm. The latter value and

a stroke of 11.5 mm (value of shaft eccentricity) can provide an appropriate course of changes in the engine working space (0.294 dm^3). Figure 8.4 shows a window with the cylinder model main parameters given, while Table 8.3 provides their values.

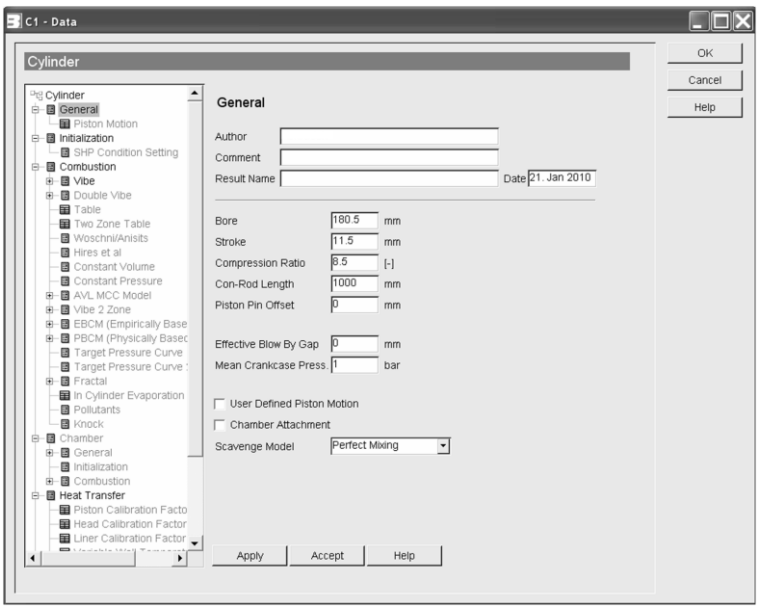

Fig. 8.4. Cylinder model

Tab. 8.3. Values of cylinder model mean parameters

parameter	value	unit
bore	180.5	mm
stroke	11.5	mm
compression ratio	8.5	-
connecting rod lenght	1,000	mm
scavenge model	perfect mixing	-

A complete Wankel engine cycle takes place in one rotor revolution. The rotor rotates at a speed three times less than crankshaft speed. It means that for a working cycle there are three (1,080º CA) and not two crankshaft rotations (720° CA) just as in 4-stroke piston engines. Consequently, the data entered into the model, e.g. timing angle and any calculation results should be appropriately scaled. For example, to ensure the engine operating conditions at a speed of 9,000 rpm, a simulation needs to be done for a speed of 6,000 rpm. Any values of quantities dependent on speed like engine effective power should be recalculated.

The Wankel engine charge is exchanged by exposing and covering channels with the rotor edge. To model a change in the cross-section of inlets and outlets, the function to control charge exchange with a piston edge is applied, and cross-sectional characteristics as a function of a crankshaft angle is used (Figure 8.5).

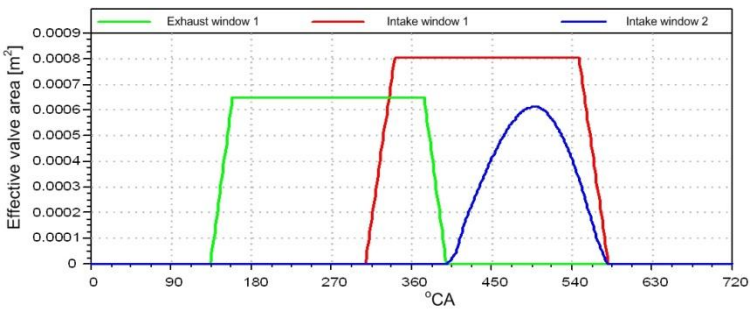

Fig. 8.5. Engine timing as a function of a crankshaft angle

The next step in modelling is to define the parameters for the heat exchange between a working medium and the engine working elements. The window with the cylinder model heat exchange is in Figure 8.6, while the values of the parameters are in Table 8.4.

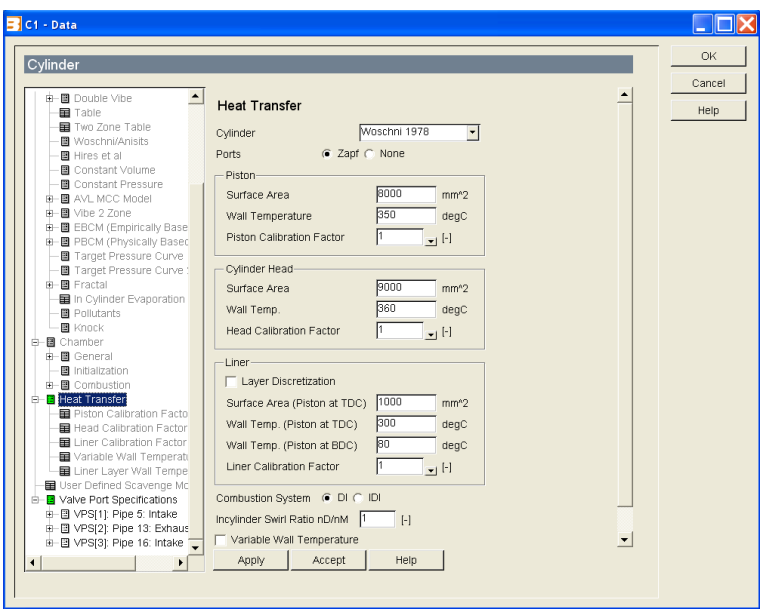

Fig. 8.6. Cylinder heat exchange model

Tab. 8.4. Values of heat exchange parameters in the cylinder model

function	symbol	quantity
system boundary	SB	2
restriction	R	11
injector	I	1
measurment point	MP	3
air cleaner	AC	1
cylinder	C	3
plenum	P	5
3D cell general	3DG	1
throttle	TH	2
connection	-	35

The final step is to define engine friction which is determined in BOOST by mean friction pressure. Its value is assumed to be 0.21 MPa for an effective pressure of 1 MPa and a speed of 2,000 rpm, while 0.24 MPa for a speed of 7,000 rpm.

8.5. Model calibration

The model is calibrated by comparing the calculated torque with the external characteristics obtained experimentally. As a result, the main simulation parameters are set up in the window of Simulation Control. The combustible mixture produced in the intake pipe is assumed to have a stechiometric composition. The type of fuel, i.e. petrol is also defined. The calculations are done for nine speed values (Figure 8.7, Case Explorer). To determine effective pressure, simulation time is assumed to cover 15 operation cycles.

The calculations done result in the characteristics of engine torque. The results of the simulation and experimental studies are compared in a common graph (Figure 8.8). The course of the torque shows that the model can map a real engine properly. The maximum calculation error for the torque amounts to 11%, and it does not exceed 5% for most measurement points (Figure 8.9). The shape of the torque curve is similar, too.

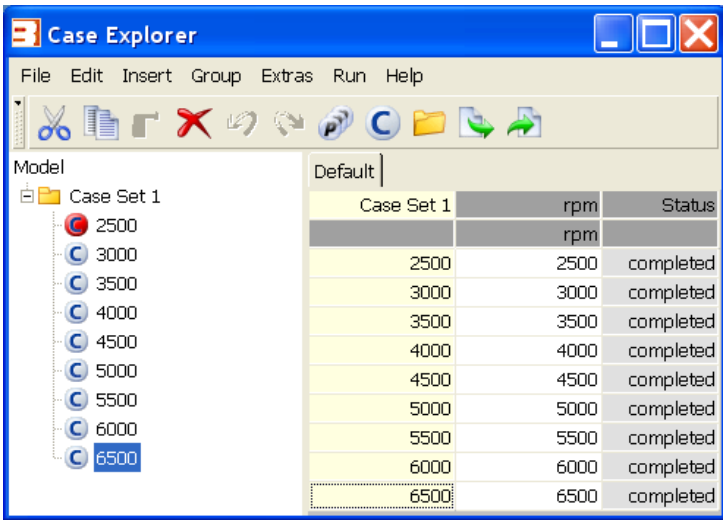

Fig. 8.7. Case Explorer window

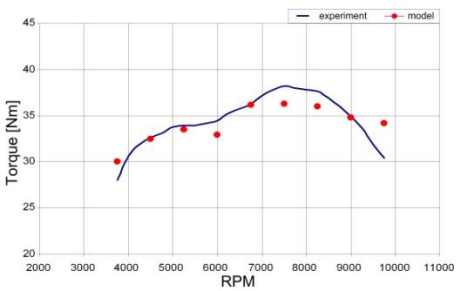

Fig. 8.8. Characteristics of the torque for the XR50 engine to verify the model

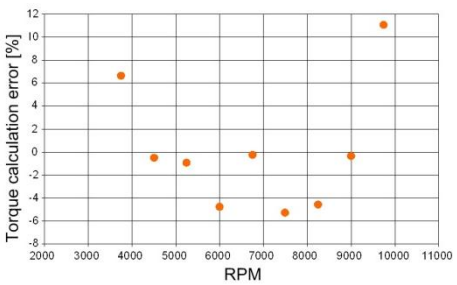

Fig. 8.9. Torque calculation error

8.6. Conclusion

These results confirm that using the AVL BOOST software to simulate a Wankel engine is a correct choice. While using the software components available only, the results obtained are satisfactory, which is supported by a calculation error of 5%. Nevertheless, some further calibration is planned to reduce this error. The next research phase involves using a hydrogen fuel injection for this model. This will allow engine performance to be initially specified followed by fuel changing.

References

[1] Anderson P.: *Intake Air Dynamics on a Turbocharged SI-Engine with Wastegate*. Departament of Electrical Engineering, Linköping University, Linköping, 2002.

[2] Batteh J., Tiller M., Newman Ch.: *Simulation of Engine Systems in Modelica*. 3rd International Modelica Conference, November 3-4, 2003, Simulation of Engine Systems in Modelica, pp. 139-148.

[3] Fischer R., Fraidl G., Hubmann Ch., Kapus P., Kunyeman R., Sifferlinger B., Beste F.: *Range Extander Module Ennablet for Electric Mobility*. ATZ auto technology, October 2009, vol. 9, pp. 40-47.

[4] Fontana G., Galloni E., Palmaccio R., Strazzullo L. Vittorioso G.: *Development of a New Intake System for a Small Spark-Ignition Engine. Modeling the Flow Through the Inlet Valve*. SAE Technical Paper nr 2003-01-0369, 2003.

[5] Izweik H. T.: *CFD Investigations of Mixture Formation, Flow and Combustion for Multi-Fuel Rotary Engine*. Technischen Universität Cottbus, 2009.

[6] Jerrelind J.: *A Study in Model Based Control of an Evaporative Emission Management System*. Tekniska Högskolan in Linköping, 1998.

[7] Jeż M., Świder A.: *Analiza drgań nieliniowych jednocylindrowego silnika tłokowego*. Journal of Kones. Combustion Engines, VoI. B, No 3-4, 2001, pp. 98-105.

[8] Kopeć S., Witek A.: *Modelowanie i analiza dynamiki zespołu wału korbowego silnika spalinowego*. Komisja Budowy Maszyn PAN – Oddział w Poznaniu, Vol. 26 nr 2, Archiwum Technologii Maszyn i Automatyzacji, 2006.

[9] Leo D. J., Nelson D. J., Ellis W. M.: *Model of the Air System Transients in a Fuel Cell Vehicle*. Master of Science in Mechanical Engineering, Blackburg, Virginia, 2002.

[10] Semin, Bakar R. A., Ismail A. R.: *Investigation of Diesel Engine Performance Based on Simulation*. American Journal of Applied Sciences 5 (6): pp. 610-617, 2008.

[11] www.fev.com.

Jacek CZARNIGOWSKI

9. The study on the hydrogen admixture in the automotive engine

Abstract

This paper reports the results regarding the modelled combustion of a petrol and HHO mixture in SI engines. HHO gas is a hydrogen and oxygen mixture which is a product resulting from the operation of an electrolyser mounted in a vehicle. The engine model employs a real object, i.e. Holden C20LE that is a 4-stroke engine with 4 cylinders and a 2 dm^3 displacement. The zero-dimensional engine model previously developed is used for modelling in the AVL BOOST programme. The tests are done for 10 different mixture compositions. The analysis focuses on mean effective pressure, volumetric efficiency, and heat emission. Also, the performances of an engine fuelled with petrol and a mixture composed of 90% of petrol and 10% of HHO are compared.

Keywords: hydrogen, a combustion engine, modelling, a zero-dimensional model

9.1. Introduction

Hydrogen as an engine fuel has many properties that may contribute to improving combustion efficiency and reducing the amount of toxic components in SI engine exhaust gases. Hydrogen has a higher ignition temperature (about 858 K) [1]. Hydrogen flame kinetic viscosity while burning is 0.61 cm^2/s, which is approximately four times higher than that of petrol (0.16 cm^2/s). This property improves the process of mixing fuel with air and helps to achieve a homogeneous mixture in a cylinder. An adiabatic hydrogen burn rate is 237 cm/s, which is five times higher than that of petrol (42 cm/s). This may cause a combustion process more stable. Due to a higher hydrogen burn rate, a combustion curve is much closer to the ideal combustion curve, which increases thermal efficiency [2]. Unfortunately, this results in increased emissions of NO_x, which prevents this solution to be applied on a wider scale [3]. Hydrogen-powered engines produce lower torque [4] for hydrogen energy density is much lower than that of petrol. Fuelling internal combustion engines by hydrocarbon fuels and supplying hydrogen in small quantities as an addition seems to be a better approach, which has positive effects [5, 6, 7].

A further advantage of hydrogen-powered engines is that they can work even if a much leaner mixture is supplied [8] because the flammability of a hydrogen

mixture in air ranges from 4.1 to 75% and is much higher than that of petrol (1.5-7.6%).

In the literature, there are studies on the impact of hydrogen fuel enhancement on the duration of combustion [9]. Another important aspect of burning a hydrogen-enhanced hydrocarbon fuel is a level of toxic emissions. The authors [10] claimed that the emissions of NO_x, HC and CO decreased following hydrogen enhancement as compared to those in an original engine.

The authors [11] studied the impact of hydrogen enhancement on the efficiency of a petrol SI engine at idle and a stoichiometric mixture and claimed that effective indicative pressure reduced steadily when hydrogen was added.

Furthermore, HHO enhancement increases the amount of oxygen in a mixture. The research conducted in the Argonne National Laboratory [5] by the researchers from the University of Chicago confirmed that the emission of CO, CO_2, and HC decreased in exhaust gases because of oxygen-enriched air under varied load conditions.

9.2. Research methodology

Many papers describe engine physical modelling [3, 12]. It is clear that zero-dimensional modelling based on the principle of mass and energy conservation in the entire modelled element is much faster than three-dimensional modelling so the author has chosen the former method to be used in the AVL BOOST programme.

To model the combustion of petrol-hydrogen-air mixtures, a cylinder hydrogen fuel mass shares are modified (Table 9.1). For the engine is powered by HHO added, this electrolyzer-generated gas is assumed to have 33.33% of oxygen and 66.66% of hydrogen. The tests were done for full engine load and two values of speed, i.e. 2,500 and 5,000 rpm. The engine outer characteristics for two extreme gas-hydrogen mixtures are developed.

Tab. 9.1. Fuel mass compositions

No.	petrol	H_2	O_2
1	0.9	0.067	0.033
2	0.1	0.060	0.030
3	0.92	0.053	0.027
4	0.93	0.047	0.023
5	0.94	0.040	0.020
6	0.95	0.033	0.017
7	0.96	0.027	0.013
8	0.97	0.020	0.010
9	0.97	0.013	0.007
10	0.99	0.006	0.004

9.3. Research object

The engine tested is the C20LE Holden 4-stroke engine with four in-line cylinders, a displacement of 1998 cm^3, and a compression ratio of 8.8:1 (Fig. 9.1). The engine has got a multipoint fuel injection into an intake manifold. Its selected parameters and the data regarding sensors and actuators in the engine control system are given in Table 9.2 and 9.3, respectively.

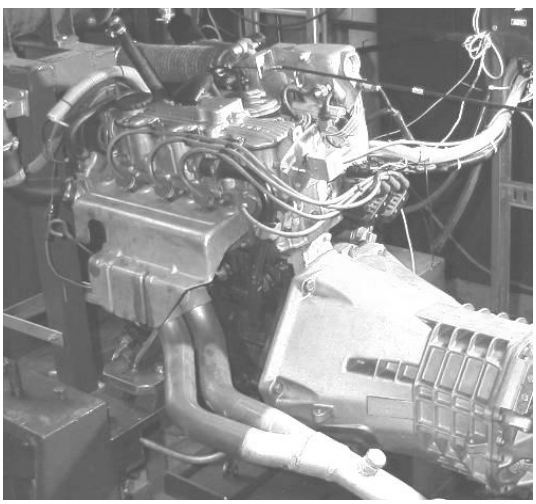

Fig. 9.1. Research object

Tab. 9.2. Holden engine specifications

parameter	value and unit
manufacturer	Holden
engine symbol	C20LE
model	2.0 MPFI
type	4-stroke, SI
cylinder number and configuration	4, in-line
bore and stroke	86/86 mm
capacity	1998 cm^3
compression ratio	8.8:1
max. engine power	77 kW at 5,200 rpm
max. torque	164 Nm at 2,600 rpm
rotation at idle	800 ±50 rpm
cylinder sequence	1-3-4-2
ignition type	Direct Ignition System - DIS module

Tab. 9.3. Sensors and actuators in the control system

measurement sensors	actuator systems
crankshaft position sensor	injectors (4)
throttle position sensor	ignition system (DIS)
coolant temperature sensor	fuel pump
inlet manifold temperature sensor	stepper motor for an air control valve
oxygen sensor (lambda sensor)	
velocity sensor (mounted in a gear box)	

9.4. AVL BOOST engine modelling and research scope

The author used this software to model the object described in Section 9.3, using the following elements:

- an intake system with an air filter,
- cylinders,
- an outlet system with a catalytic exhaust gas treatment system,
- petrol injectors.

To obtain a mixture of petrol-hydrogen-air, he used this function to determine the composition of gases in a cylinder. Figure 9.2 shows the complete engine model.

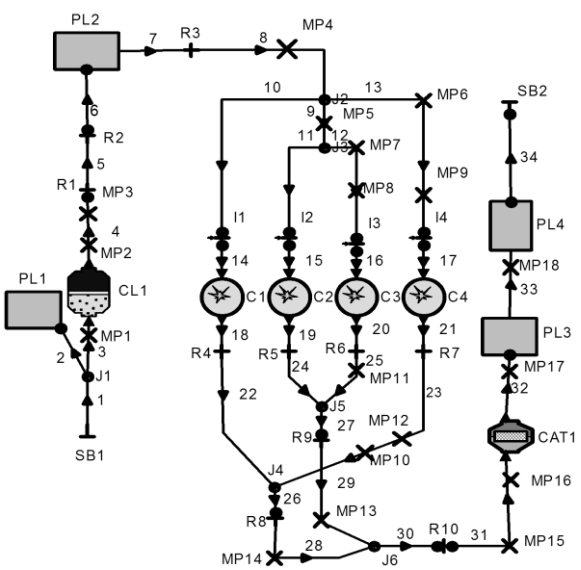

Fig. 9.2. AVL BOOST engine model

The engine modelling is based on standard components available in the software libraries so it was necessary to simplify the engine construction, as shown in Table 9.4.

Tab. 9.4. Modelling functions

function	symbol	quantity
system boundary	SB	2
restriction	R	10
injector	I	4
measurement point	MP	18
air cleaner	AC	1
cylinder	C	4
plenum	P	4
connection	-	34
catalist	CAT	1

9.5. Results

Figures 9.3-9.5 present the test results regarding an engine powered with a petrol and HHO mixture and petrol. All the dependencies are for full engine loading.

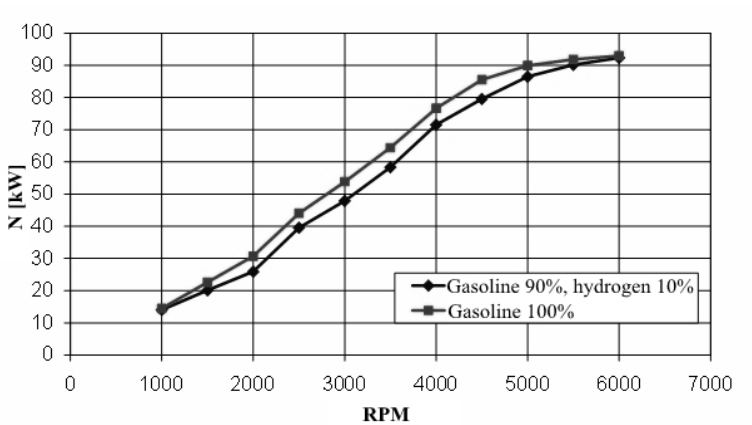

Fig. 9.3. Power depending on rotation velocity for the two extreme mixture compositions

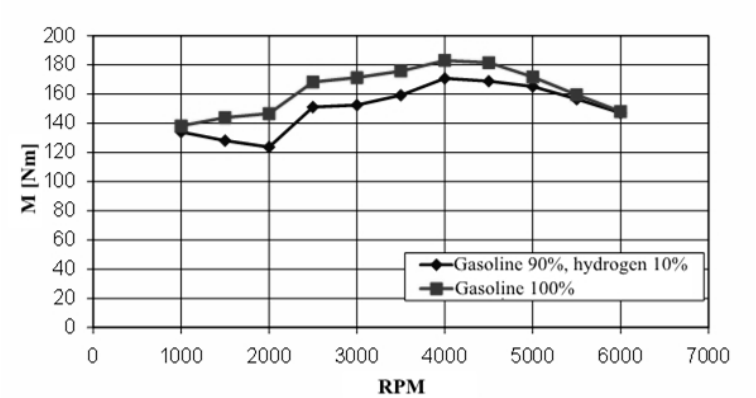

Fig. 9.4. Torque depending on rotation velocity for two extreme mixture compositions

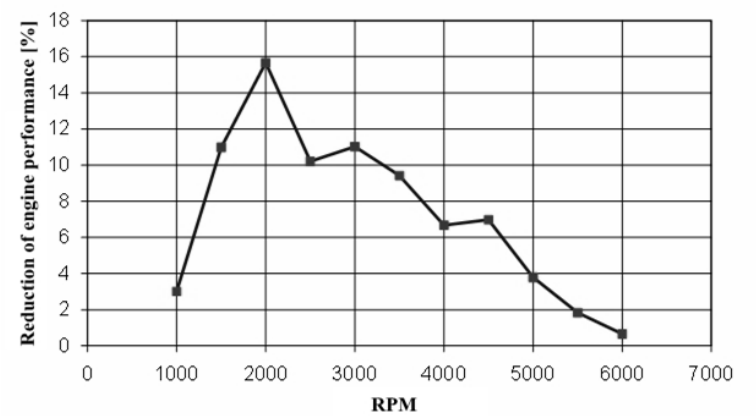

Fig. 9.5. Reduced engine performance depending on rotation velocity

Based on the chart with full engine power for the two fuels (Fig. 9.3), the reduced power can be noticed, which results from supplying the engine with a mixture of hydrogen and oxygen. The most significant discrepancy is for 2,000 rpm, while the most negligible, i.e. about 3% is for 1,000 and 6,000 rpm. The changes in torque are similar (see Fig. 9.4).

This tendency is due to a change in the volumetric efficiency of the object tested. The best filling efficiency is for 4,500 rpm, and the worst one is for 2,000 rpm.

Figures 9.6-9.9 present the modelling results for varied mixture compositions. The further figures refer to the mean effective pressure, combustion chamber heat and carbon dioxide concentration. The simulations are done for 5,000 rpm.

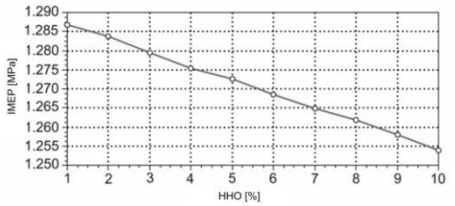

Fig. 9.6. Mean effective pressure depending on the mass share of a hydrogen-oxygen mixture

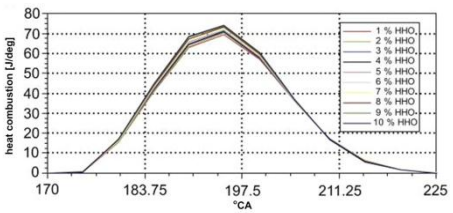

Fig. 9.7. Heat emission in the combustion chamber for varied mixture compositions

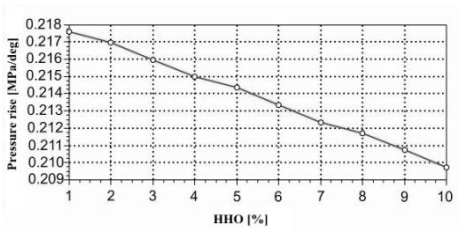

Fig. 9.8. Pressure rise in the cylinder depending on mass share of a hydrogen-oxygen mixture

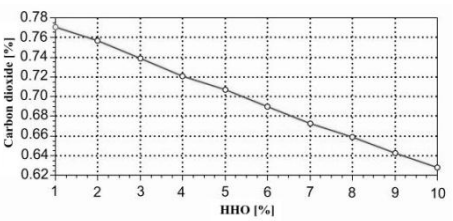

Fig. 9.9. Carbon dioxide concentration in the exhaust gases on the mass share of a hydrogen-oxygen mixture

Figure 9.6 shows the decreasing mean effective pressure by about 0.03 MPa after HHO is added. Figure 9.7 shows heat release. It can be noticed that the higher share of hydrogen and oxygen in the mixture increases heat release by about 6 J/^{o}CA and a chamber pressure increasing rate decreases by about 0.01 MPa/^{o}CA (Fig. 9.8). Figure 9.9 shows that the increased mass share of HHO reduces the mass concentration of carbon dioxide in the exhaust gases by about 7%, which results from the decreased mass share of coal in fuel and supplied oxygen.

9.6. Conclusion

The following conclusions can be formulated based on modelling petrol-hydrogen-air mixture combustion:

- hydrogen-oxygen mixtures in a combustion chamber can significantly affect combustion,
- they reduce toxic compounds in exhaust gases, e.g. carbon dioxide and nitrogen oxides, in particular,
- the increased share of hydrogen and oxygen (HHO mixtures) in a combustion chamber reduces mean effective pressure and is accompanied by reduced engine performance,
- the changes in heat release and a pressure increasing rate and a shift in maximum pressure are recorded.

References

[1] Das L. M.: *Hydrogen–oxygen reaction mechanism and its implication to hydrogen engine combustion*. International Journal of Hydrogen Energy, 1996;21:703–15.

[2] Ma F., Wang Y., Liu H., Li Y., Wang J., Ding S.: *Effects of hydrogen addition on cycle-by-cycle variations in a lean burn natural gas spark-ignition engine*. International Journal of Hydrogen Energy, 2008;33:823–31.

[3] Leo D. J., Nelson D. J., Ellis W. M.: *Model of the Air System Transients in a Fuel Cell Vehicle*. Master of Science in Mechanical Engineering, Blackburg, Virginia, 2002.

[4] Ganeshb R. H., Subramaniana V., Balasubramanianb V., Mallikarjuna J. M., Ramesh A., Sharma R. P.: *Hydrogen fueled spark ignition engine with electronically controlled manifold injection: an experimental study*. Renewable Energy 2008; 33:1324–33.

[5] Akansu S. O., Kahraman N., Ceper B.: *Experimental study on a spark ignition engine fuelled by methane–hydrogen mixtures*. International Journal of Hydrogen Energy 2007, 32:4279–84.

[6] Porpatham E., Ramesh A., Nagalingam B.: *Effect of hydrogen addition on the performance of a biogas fuelled spark ignition engine*. International Journal of Hydrogen Energy 2007; 32:2057–65.

[7] Liu B., Huang Z., Zeng K., et al.: *Experimental study on emissions of a spark-ignition engine fueled with natural gas hydrogen blends*. Energy and Fuels 2008, 22:273–7.

[8] Ma F., Wang Y.: *Study on the extension of lean operation limit through hydrogen enrichment in a natural gas spark-ignition engine*. International Journal of Hydrogen Energy 2008, 33:1416–24.

[9] Andrea T. D., Henshaw P. F., Ting D. S. K.: *The addition of hydrogen to a gasoline –fuelled SI engine*. International Journal of Hydrogen Energy 2004, 29:1541–52.

[10] Li J., Guo L., Du T.: *Formation and restraint of toxic emissions in hydrogen–gasoline mixture fueled engines*. International Journal of Hydrogen Energy 1998, 23:971–5.

[11] Kahraman E., Ozcanl S. C., Ozerdem B.: *An experimental study on performance and emission characteristics of a hydrogen fuelled spark ignition engine*. International Journal of Hydrogen Energy 2007, 32:2066–72.

[12] Jerrelind J.: *A Study in Model Based Control of an Evaporative Emission Management System*. Tekniska Högskolan in Linköping, 1998.